# Downsizing among the lowest mass starforming galaxies

*Roberto Terlevich, INAOE (also at IoA, Cambridge)*
*Elena Terlevich, INAOE (also at IoA, Cambridge)*
*Jesus Lopez, INAOE*

*V Workshop Estallidos*
*Granada , March 2007*



# Introduction

- The cosmic history of star-formation can be studied in more than one way.
- Directly, one uses the universe as a time-machine and obtains the "Madau-Lilly Diagram" by direct observation and analysis of the universe as a function of distance or look-back time.
- Indirectly we can use the "fossil" or “Astroarcheology" model, analyzing the $z \sim 0$ universe as seen by (for example) SDSS and, from the numbers of stars/galaxies of different ages and metallicities, extrapolate back to earlier times.
- Also we can compute forward from the era of decoupling via computer simulations and a theoretical model normalized to the observed CBR at $z \sim 1000$.
- Amazingly, the three methods seem to agree fairly well.
- New issues like the "**downsizing**" evolution of ellipticals seem to fit into the overall picture without need for exotic physics.

# Dependence of the star formation history on galaxy mass

- How does the evolution depend on the galaxy mass?
- We have known for many years that faint, low mass galaxies on average are bluer than high mass galaxies, and have stronger star formation.
- Recently, the interest in this well established observational result has grown, and its implications have been more and more appreciated. In *all* environments, lower mass galaxies have a more recent star formation history. This implies that, on average, going to lower redshifts, the maximum luminosity/mass of galaxies with significant star formation activity progressively decreases.
- This "**downsizing effect**" might suggest an "**anti-hierachical**" history for the star formation in galaxies, which parallels a similar effect observed for AGNs .

# Downsizing

Recent results suggest that the SF takes place in progressively smaller galaxies as time goes on (e.g., Heavens et al. 2004(MOPED collaboration), Bouche & Lowenthal 2005, Juneau et al. 2005, Le Borgne et al. 2005, Shapley et al. 2005,……)

Bundy, Ellis & Conselice (2005) argue that downsizing also proceeds from early to late Hubble types.

# MOPED collaboration results. Based on stellar population analysis in local galaxies, i.e. fossil method

"Local" Madau-Lilly diagram

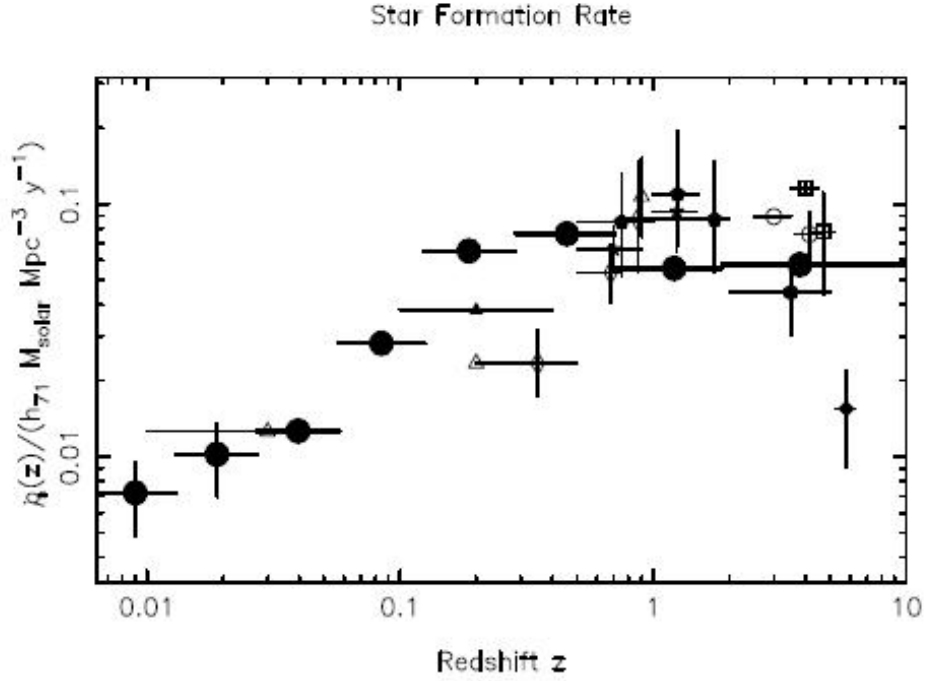



Figure 1: The star formation history of the Universe. The star formation rate recovered from the "fossil record" in the SDSS is shown by the eight large filled circles. The horizontal error bars represent the size of the bin in redshift. Vertical errors are bootstrap errors, and are invisibly small for most bins. The other symbols correspond to independent determinations using instantaneous measurements of the star formation rate, as follows; $H\alpha$ measurements are open triangles at $z \simeq 0.03$[1], $z \simeq 0.2$[5], $z \simeq 0.9$[6]; UV from Subaru[11] (open squares), GOODS[12] (filled diamond), HST etc[3] (open circles), CFRS[2] (open diamonds), HDF[4] (filled pentagons), galaxies[7] (stars), galaxies[8] (filled triangle). The filled hexagon at $z = 3.5$ represents a new estimate of the star-formation density provided by sub-mm galaxies in the redshift range $2 < z < 5$. This was derived by integrating the sub-mm source number counts[9] down to $S_{850\mu m} = 1$ mJy, and assuming that 75% of such sources lie at $z > 2$ (in line with recent redshift measurements[10]). In general the agreement is very good. However, there are two important results in our study which result from the extremely small vertical error bars. First, we find that 26% of the mass of stars in the present-day Universe were formed at $z > 2$. Second, while we confirm the previous measurements of a generally high level of star-formation activity at $z \simeq 1$, we find that global star-formation density peaked at significantly lower redshifts than previously claimed, in the bin spanning the redshift range $0.3 < z < 0.8$. The reason for this difference is clarified in Figure 2. $h_{71}$ is the Hubble constant in units of 71 $\mathrm{km\,s^{-1}\,Mpc^{-1}}$.

# MASS-DEPENDENCE IN THE MADAU-LILLY DIAGRAM

MOPED collaboration results. Based on stellar population analysis in local galaxies, i.e. Astroarcheology

Two effects are evident:

First, the SF history is very different for galaxies of different masses. Massive ones evolved much faster than lower mass ones.

Second, on average massive galaxies are older than low mass galaxies. This result applies to masses larger than $10^{10}$ Msun.

We have extended this result to the starforming galaxies with the lowest masses

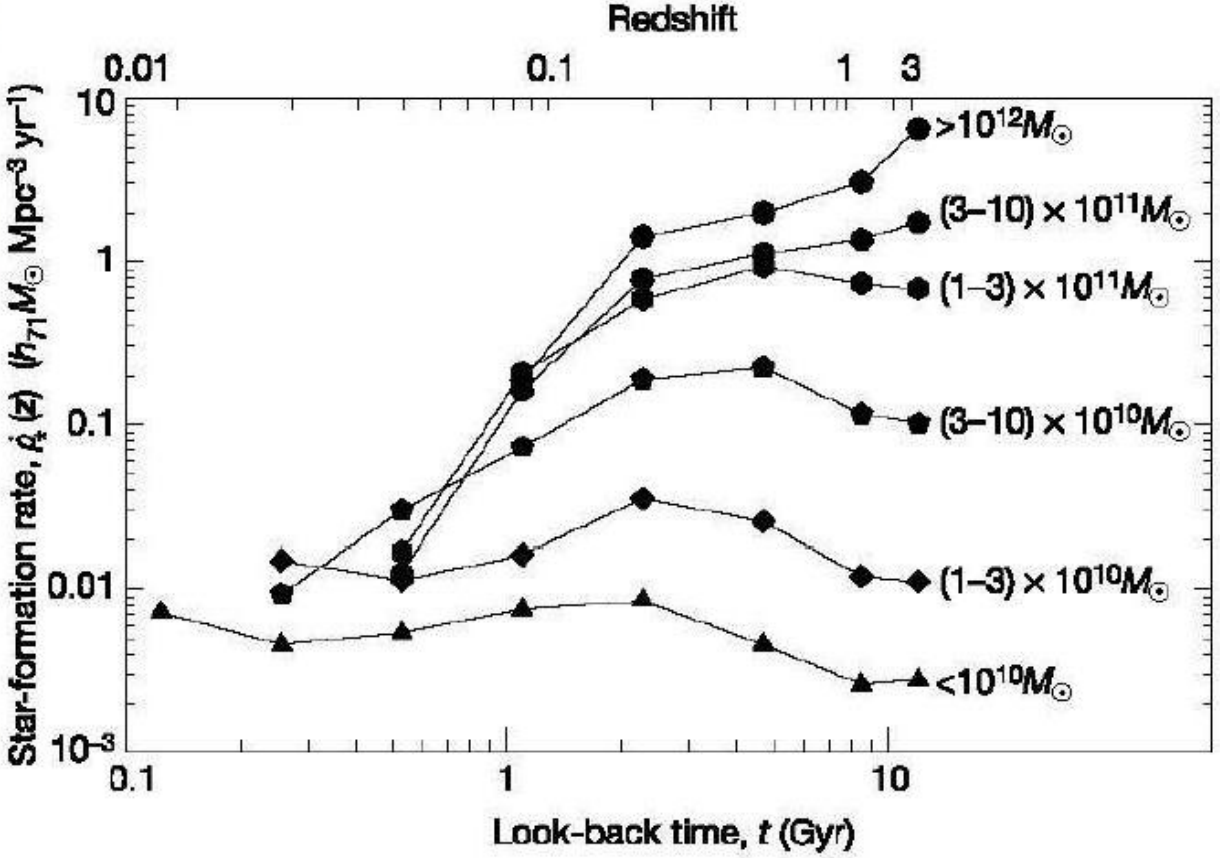



Figure 4.18: SFR vs. lookback time as a function of the galaxy mass (from (Heavens et al., 2004)).

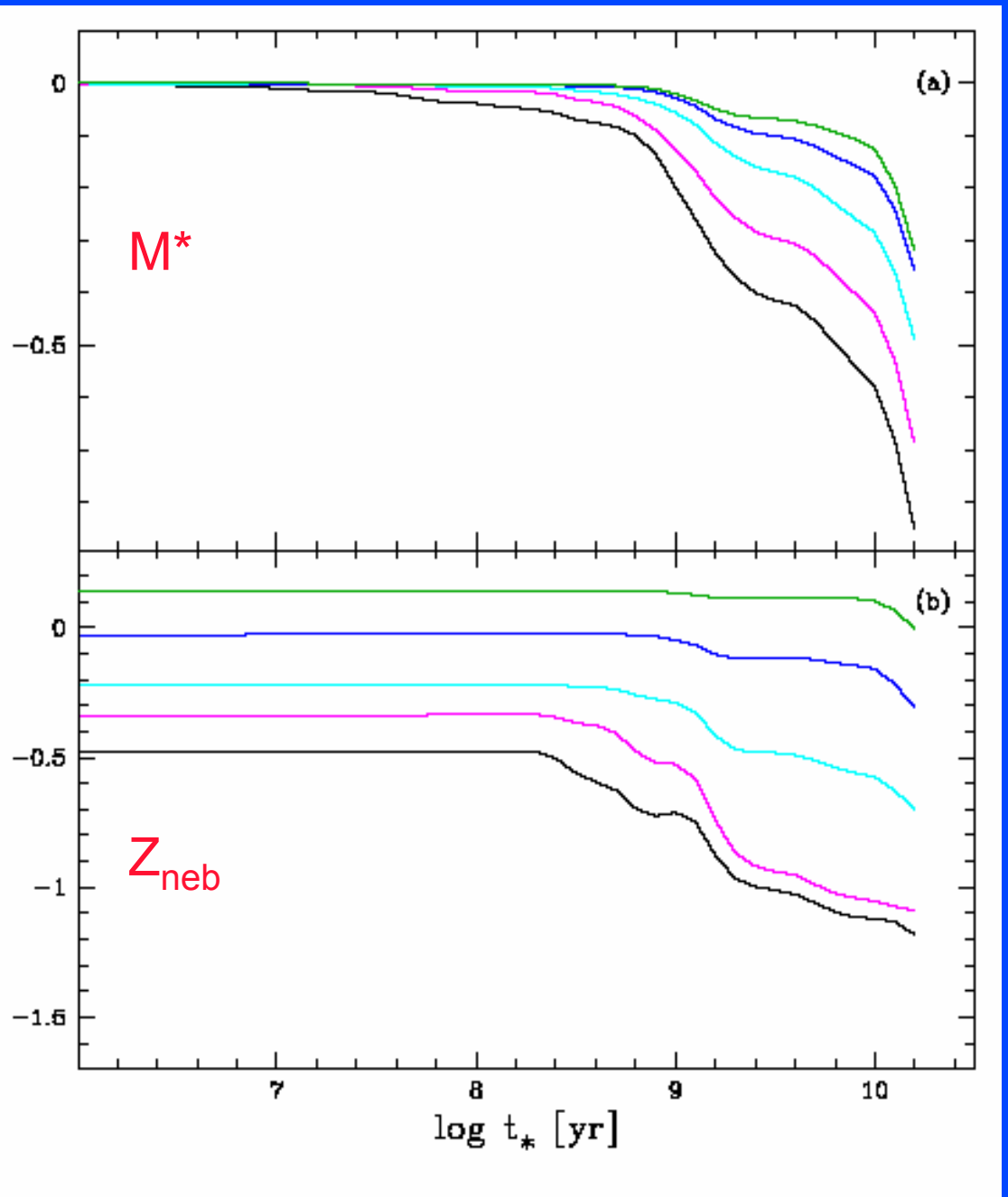
# Mass assembly history and chemical enrichment of star forming galaxies

Cid Fernandes, Asari, Sodre, Stasinska et al 2006, MNRAS

**Method of analysis of the SDSS spectra**

- **~600000 galaxies from the SDSS DR5**
- **the spectra are analyzed with the STARLIGHT code, being decomposed in a combination of 150 simple stellar populations characterized by Z* and t***

# Mass assembly history and chemical enrichment

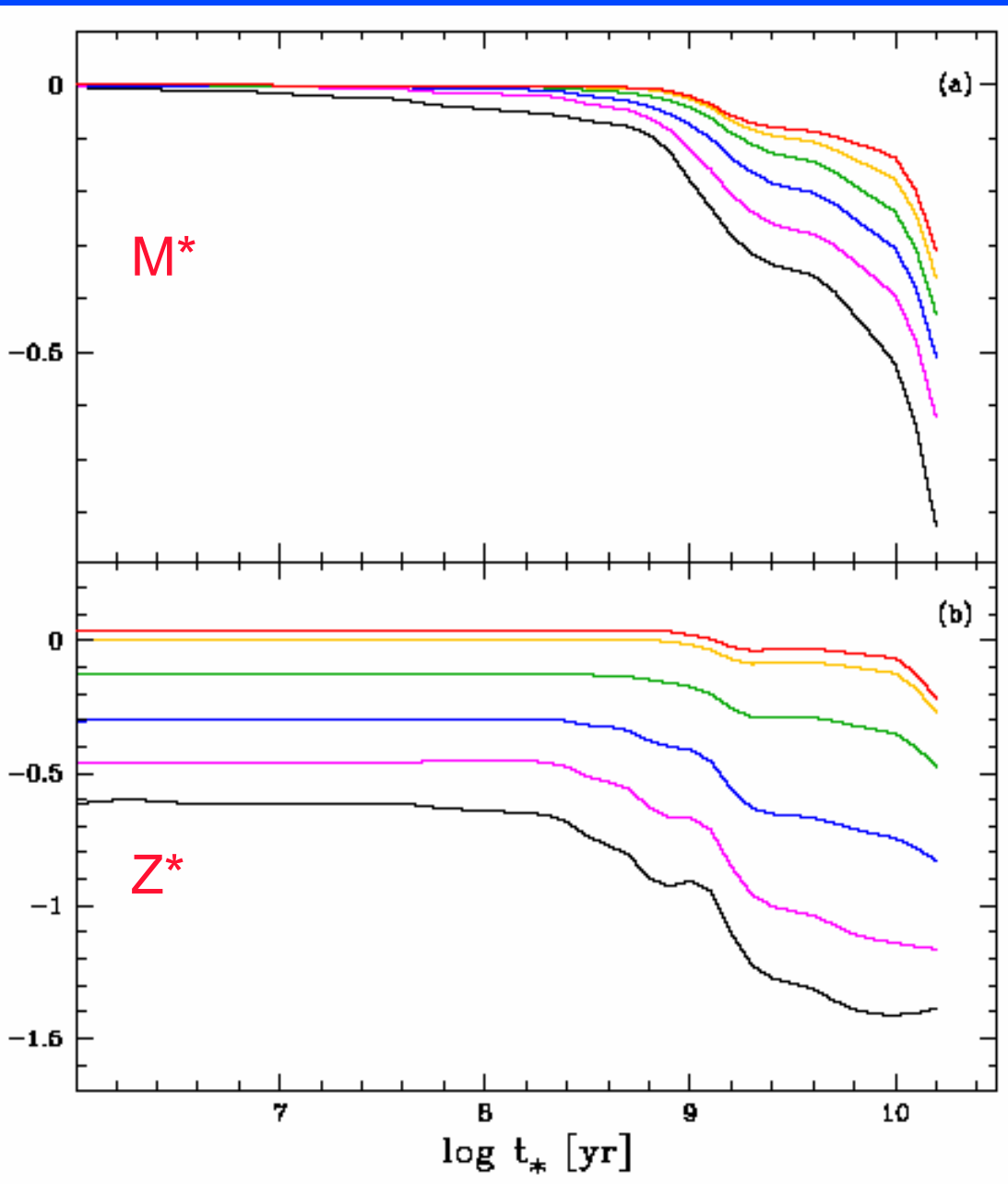


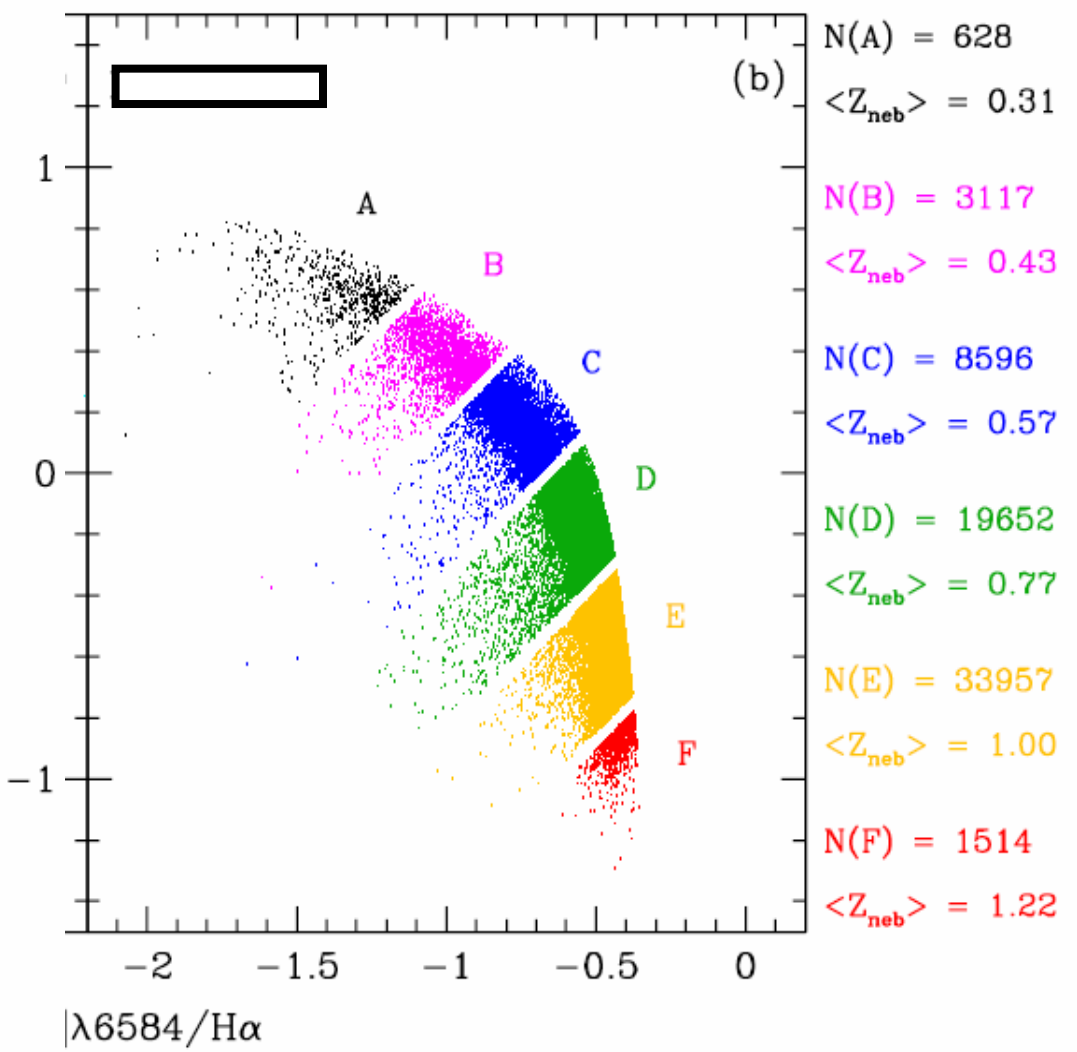

**Galaxies are binned by total stellar mass**

- **high M* systems (top curves) have completed their mass assembly and chemical enrichment long ago**
- **low M* systems (bottom curves) evolve slowly**

# Mass assembly history and chemical enrichment

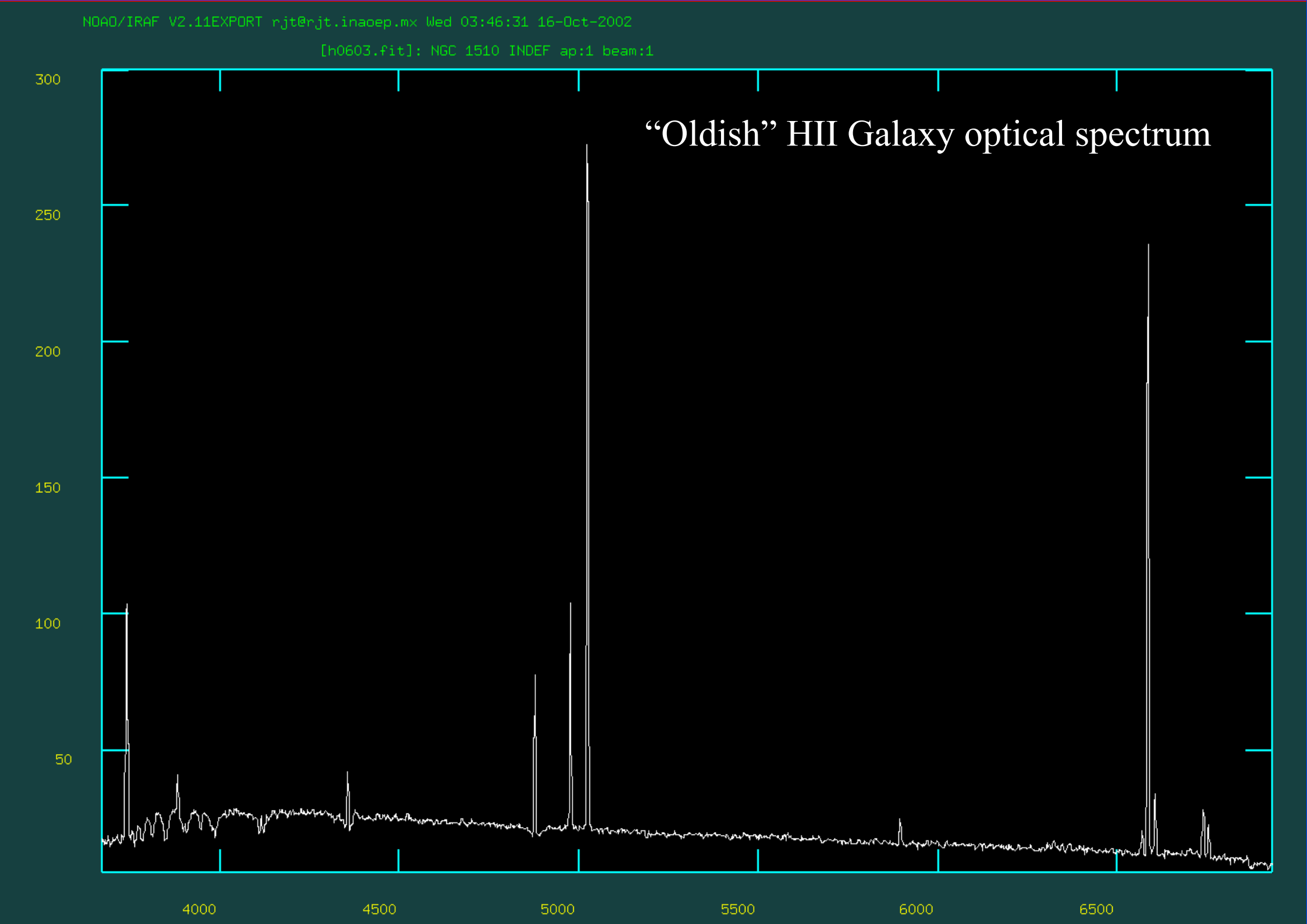
- high $Z_{neb}$ systems have completed their mass assembly and chemical enrichment long ago
- low $Z_{neb}$ systems evolve slowly



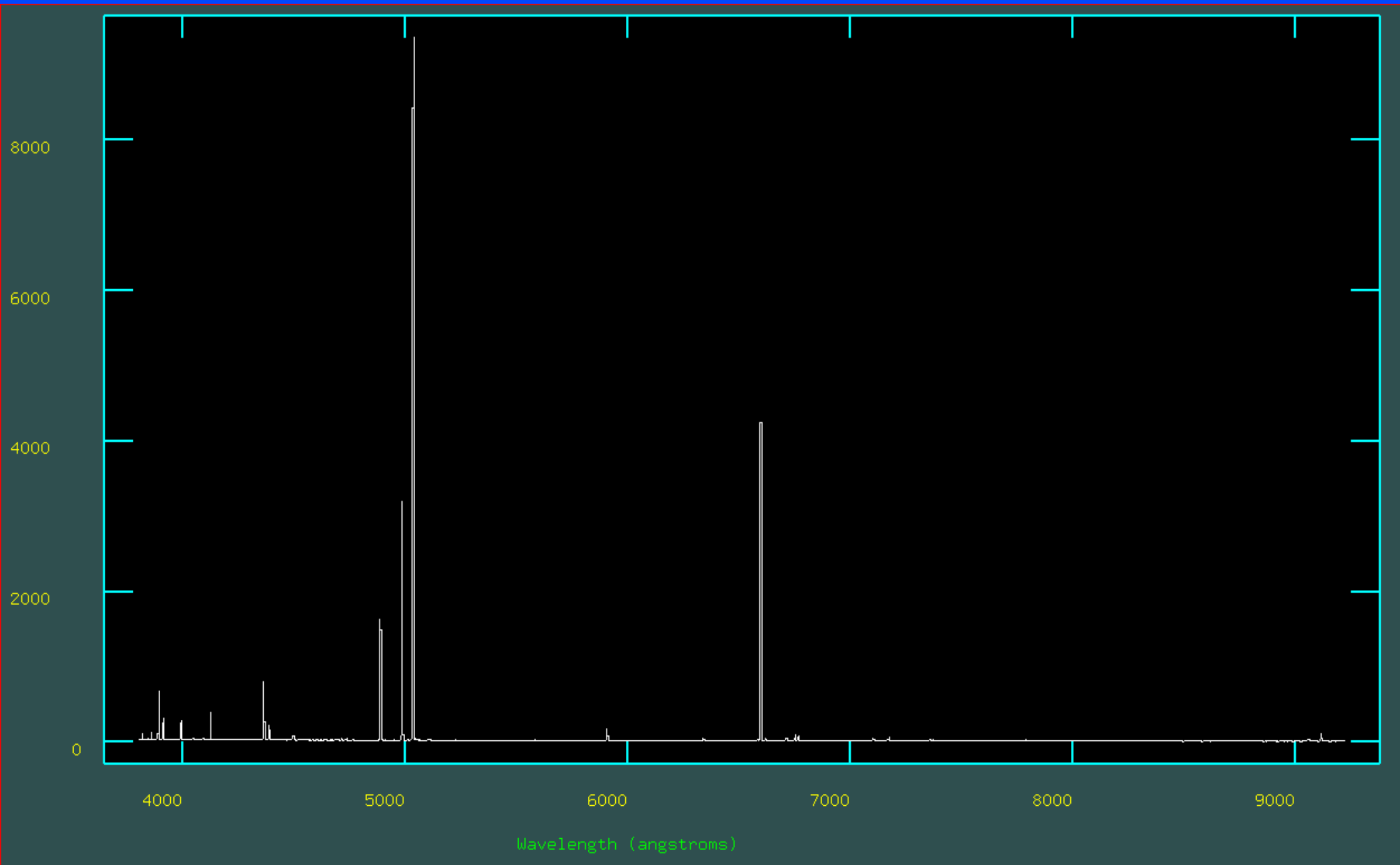



# The SF history of HII Galaxies

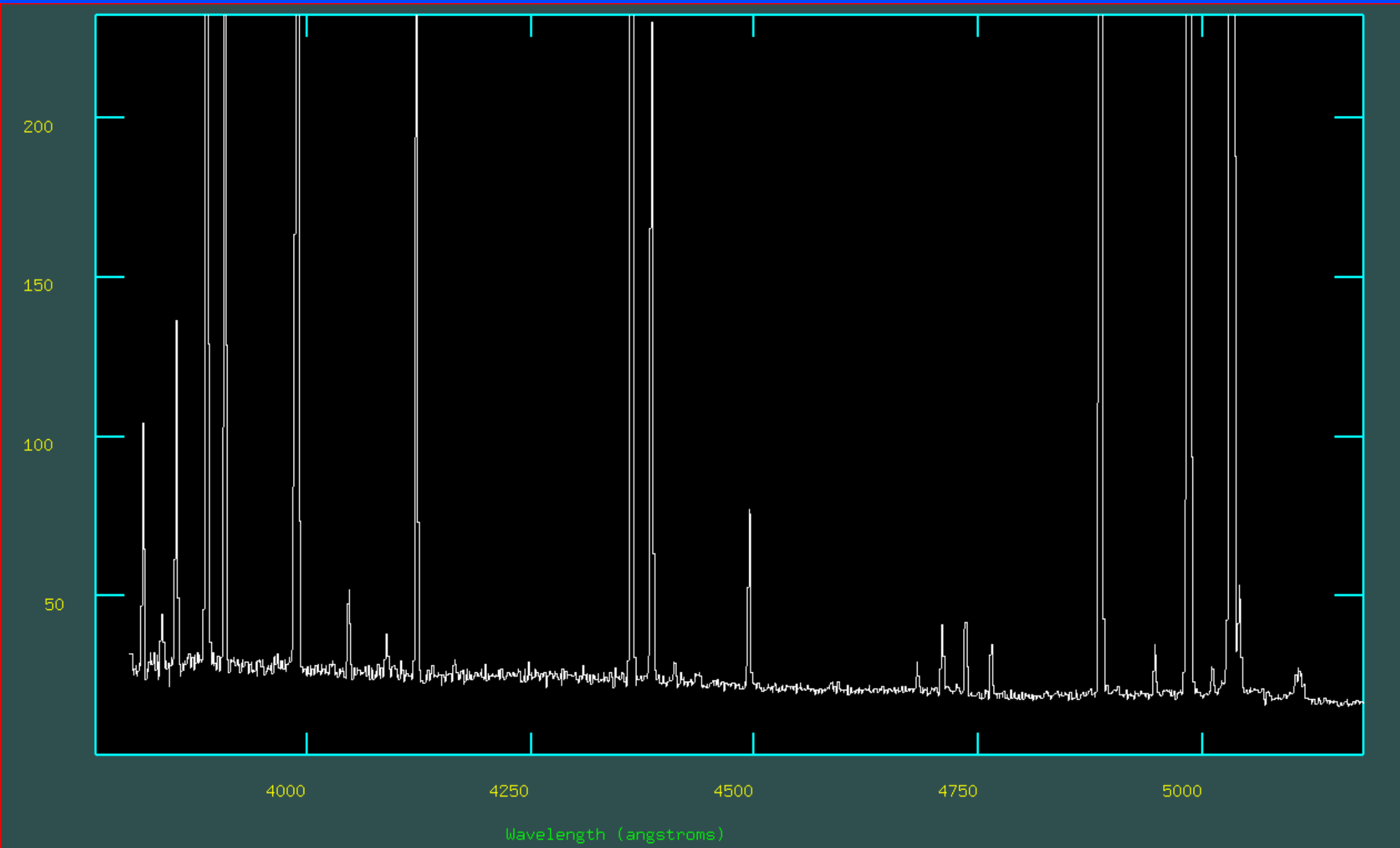
- Probably the youngest i.e. less evolved galaxies are the HII Galaxies.
- HII Galaxies are selected because their optical spectrum resembles that of Superassociations like 30-Doradus in the LMC or NGC 604 in M33.
- HII galaxies tend to be luminous and compact bursts of star formation in low mass galaxies.
- The stellar make-up indicates an extremely young stellar population.
- Their strong emission lines make them ideal for studies of chemical abundances and chemical evolution.
- Basically, HII galaxies are among the youngest stellar systems that can be studied in any detail.


NOAO/IRAF V2.11EXPORT rjt@rjt.inaoep.mx Wed 03:46:31 16-Oct-2002
[h0603.fit]: NGC 1510 INDEF ap:1 beam:1
300
250
200
150
100
50
4000
4500
5000
5500
6000
6500
"Oldish" HII Galaxy optical spectrum

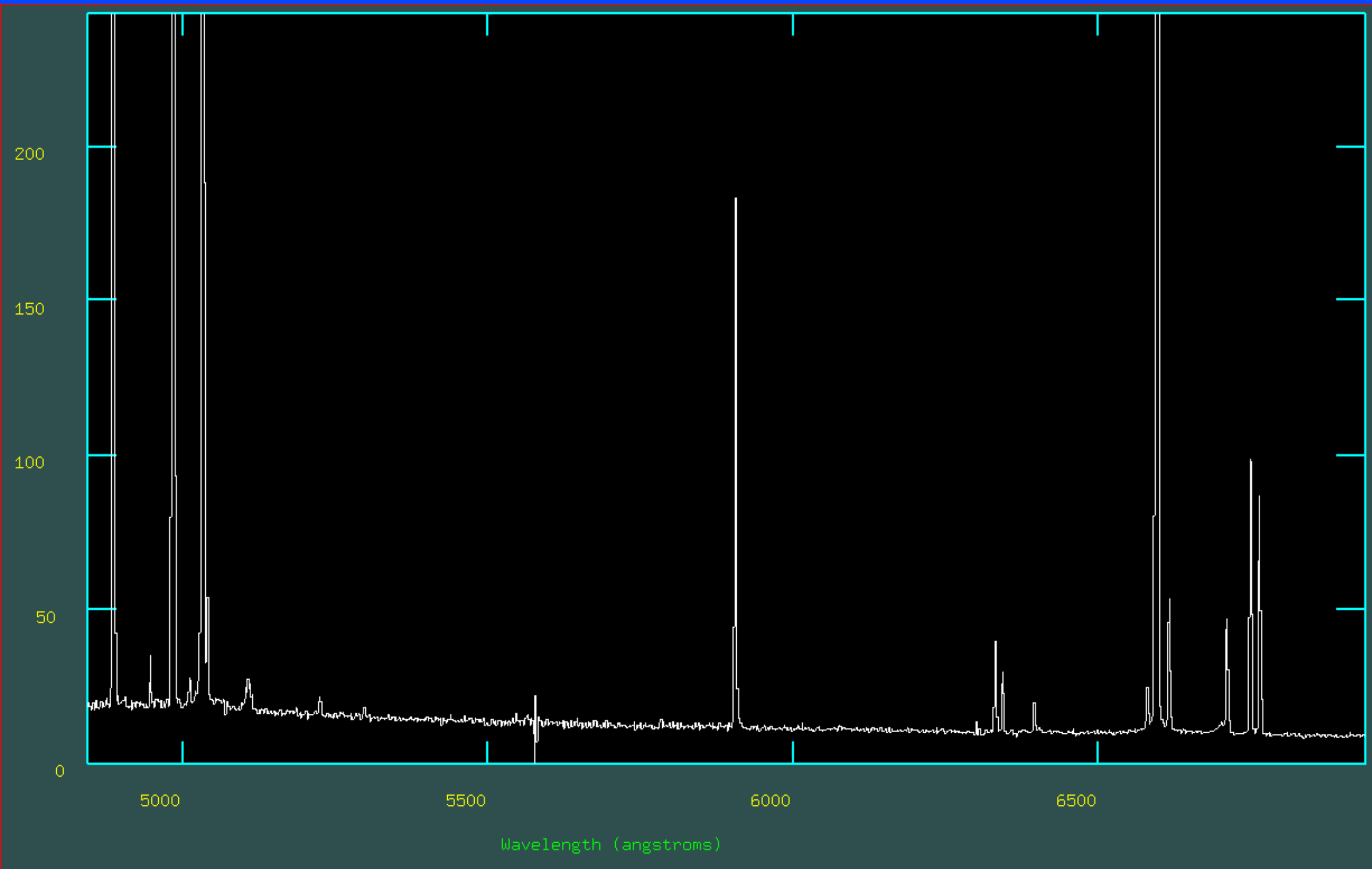
# Strong line “young” HII galaxy spectrum



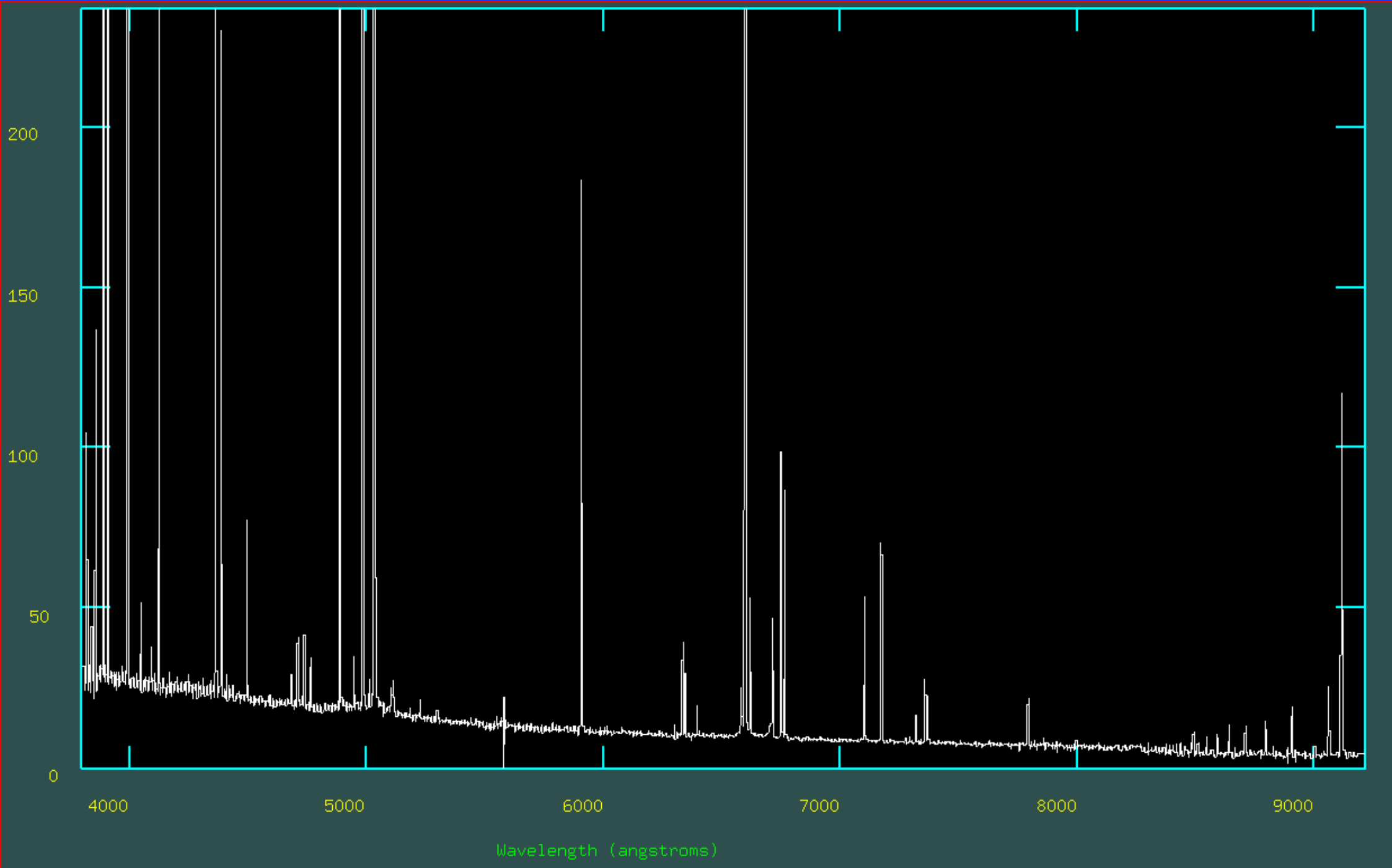
# Blue section



# Visual section



# Red-IR section



- Young stellar systems have no strong absorption lines making very difficult or impossible  the application of spectral population fit methods to determine their ages or history of star formation.

- But, emission  line methods can provide information on the ages

For many years we argued about the possible origin of the apparent lack of strong emission line systems, and the pros and cons of the different explanations without reaching a convincing case.

In collaboration with Daniel Rosa, Sergei Silich and Elena Terlevich we  developed a new approach

Terlevich etal 2004

We have shown that for a population of **independent events** that have a **monotonic evolution** , the probability density function is:

$$\rho_w(W) = -\frac{1}{t_{SF}} \frac{\mathrm{d}t(W)}{\mathrm{d}W}$$

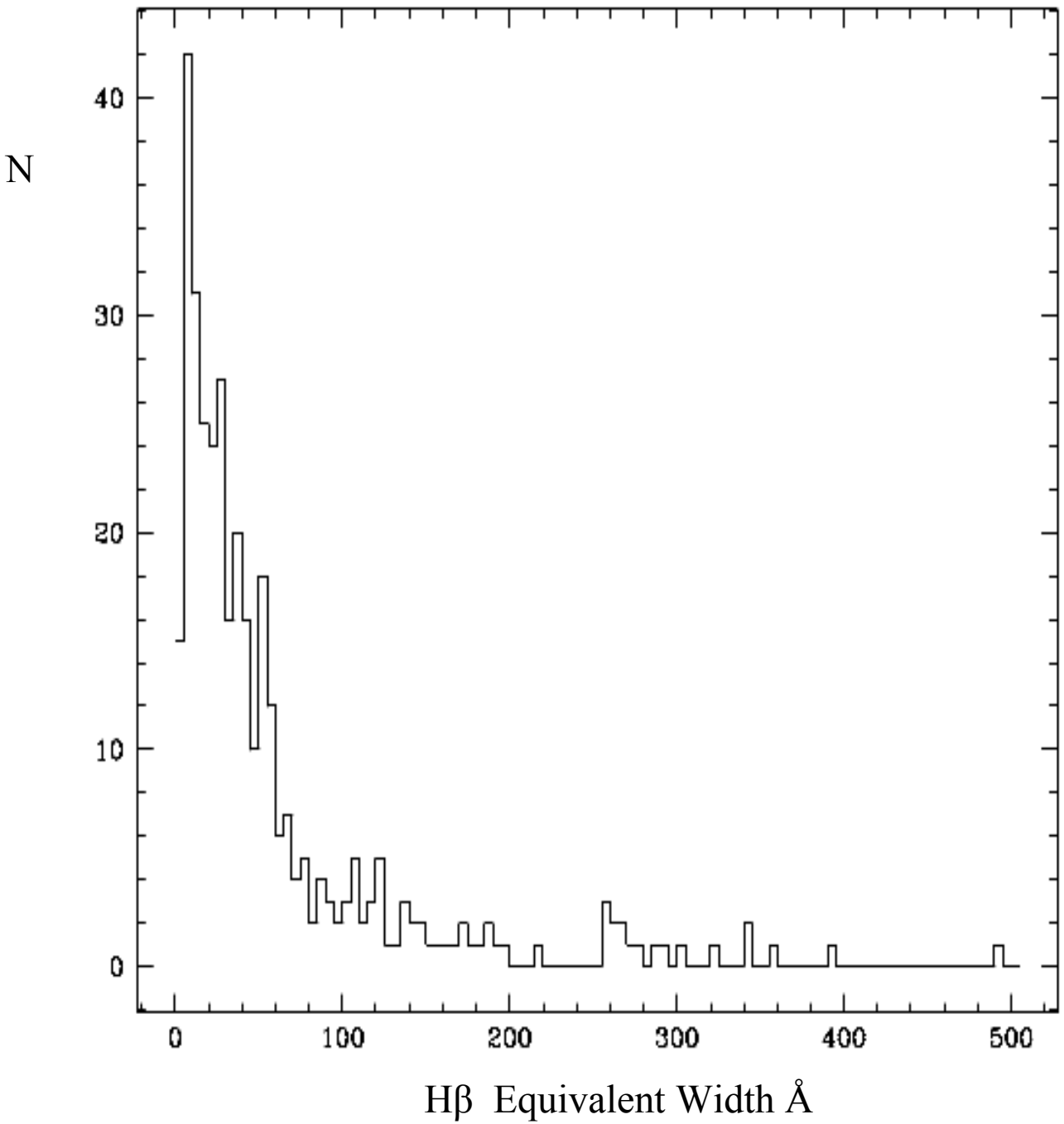
With inverse transformation:

$$t(W) = -\sum_{i_{max}}^{i} t_{SF}\, \rho_i(W)\, \Delta W = \frac{t_{SF}}{N_0} \sum_{i}^{i_{max}} \Delta N_i$$

i.e. the original distribution can be recovered

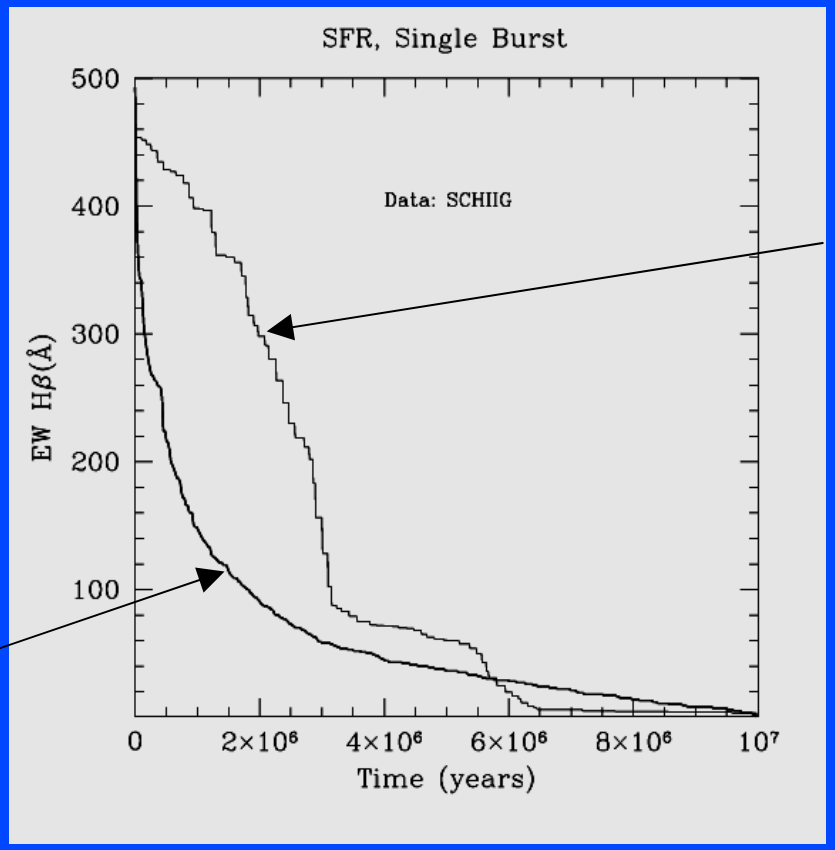
For samples of events that are randomly distributed in time, for parameters that evolve monotonically, it is possible to recover the shape of its time dependence .

The reconstructed distribution has an undetermined scale factor.




Observed distribution from the Spectrophotometric Catalogue of HII Galaxies.

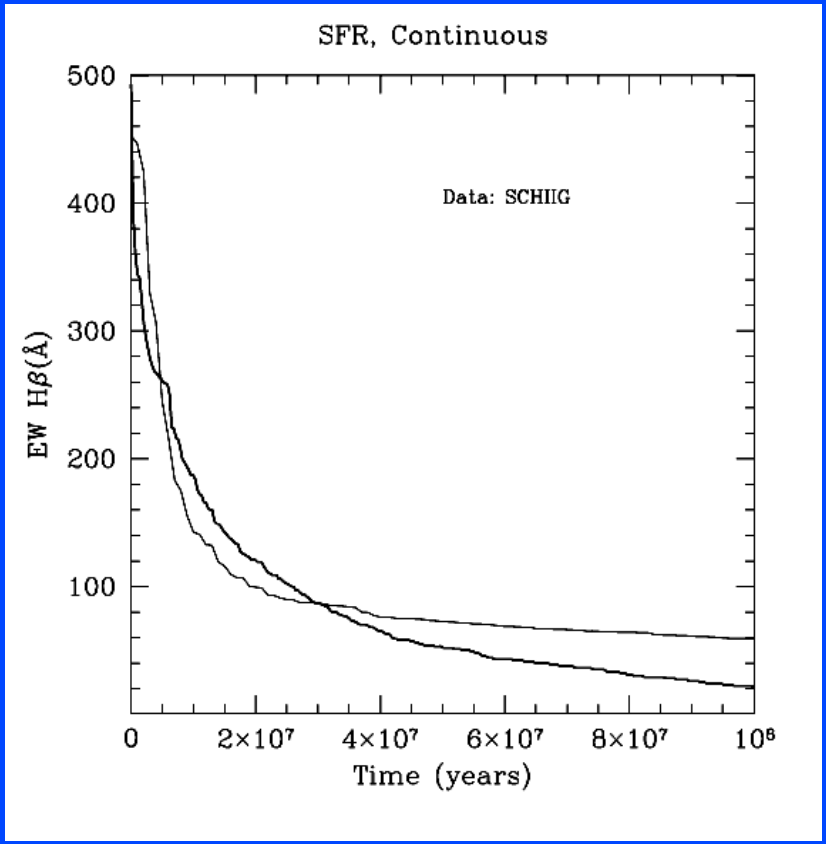
# Instantaneous SF (SCHIIG)




Model prediction

Inversion from data

# Continuous SF (SCHIIG)



Results are similar for the SCHIIGx and UCM sample and also for individual HII regions in spiral arms.

Single Burst model predictions do not fit the shape of the observed evolution of the Equivalent width of Hβ.

Continuos SFR models give a reasonably good description of the shape of the evolution of the Equivalent width of Hβ.

The conclusion is perhaps obvious:

**While the observed emission lines in HII galaxies track the present burst properties, the underlying continuum contains the whole history of SF**.

# Application to SDSS HII galaxies

- The availability of large number of good spectra of HII galaxies from SDSS prompted us to investigate the history of SF in HII galaxies for a range of masses and metallicities
- Out of more than 300,000 emission line galaxies in SDSS DR3 we have selected those with the strongest Hα emission line (EqW Hα > 100Å), giving an initial sample of about 120,000 galaxies.

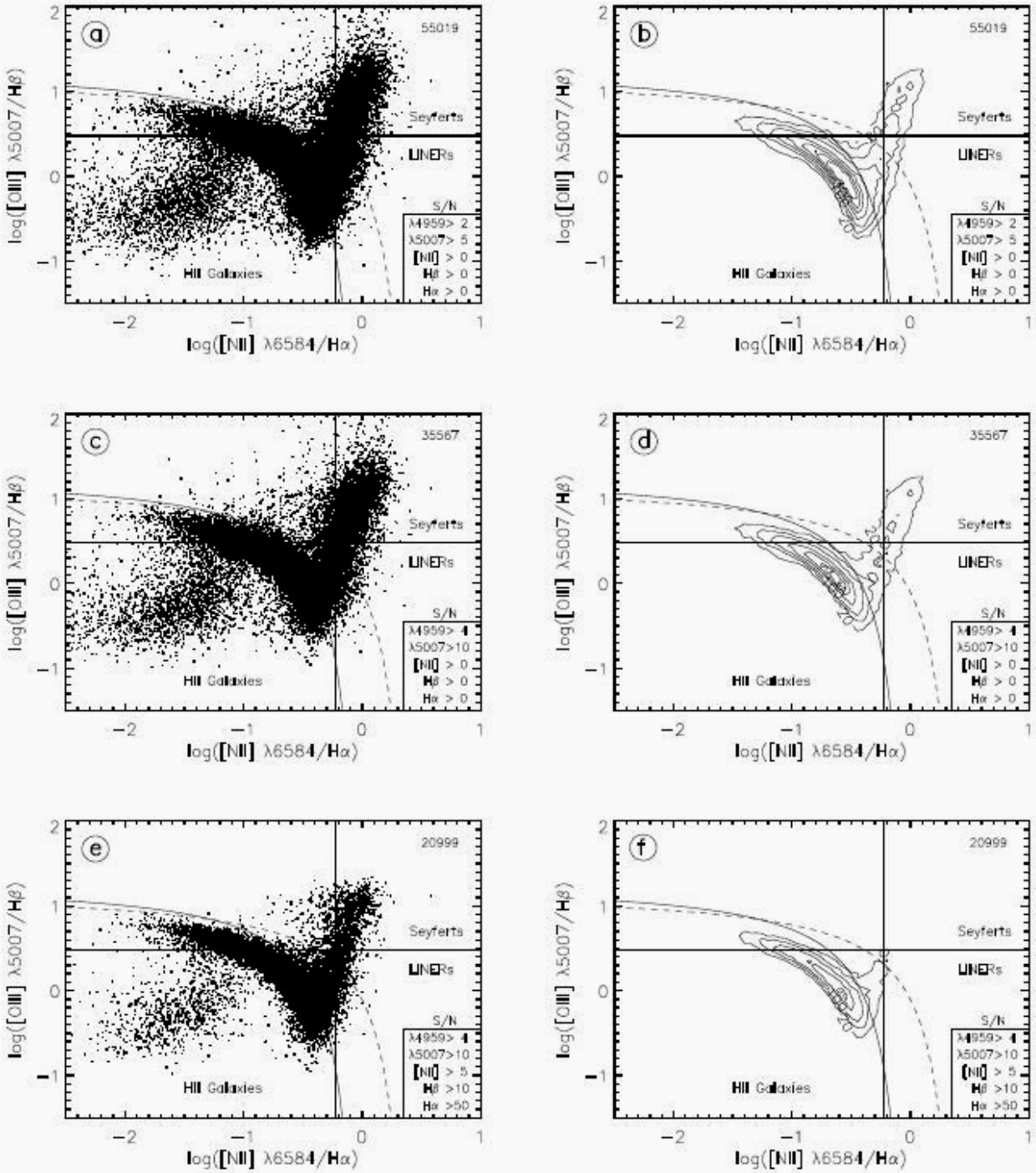



**Figure 2.9:** Diagnostic diagrams with increasing S/N restrictions. Each panel shows in the upper right corner the number of objects in the plot and in the lower right the S/N conditions.

BPT diagrams showing the effect of constraining the S/N of the data

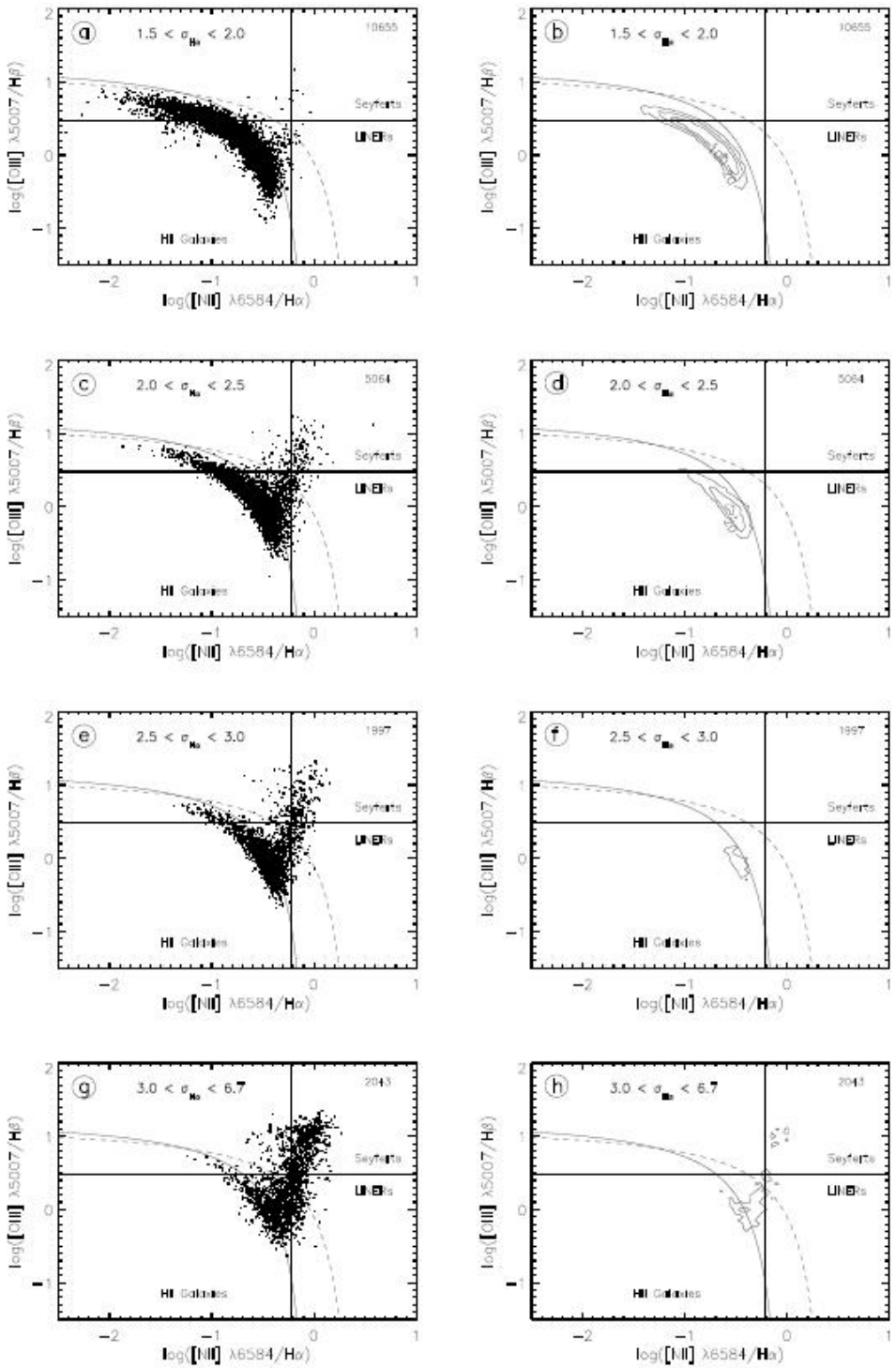



**Figure 2.12:** Use of $\sigma_{\mathrm{H}\alpha}$ as an extra parameter to reject Seyfert galaxies and LINERs

Population of the BPT diagram for different emission line widths

# Excluded objects

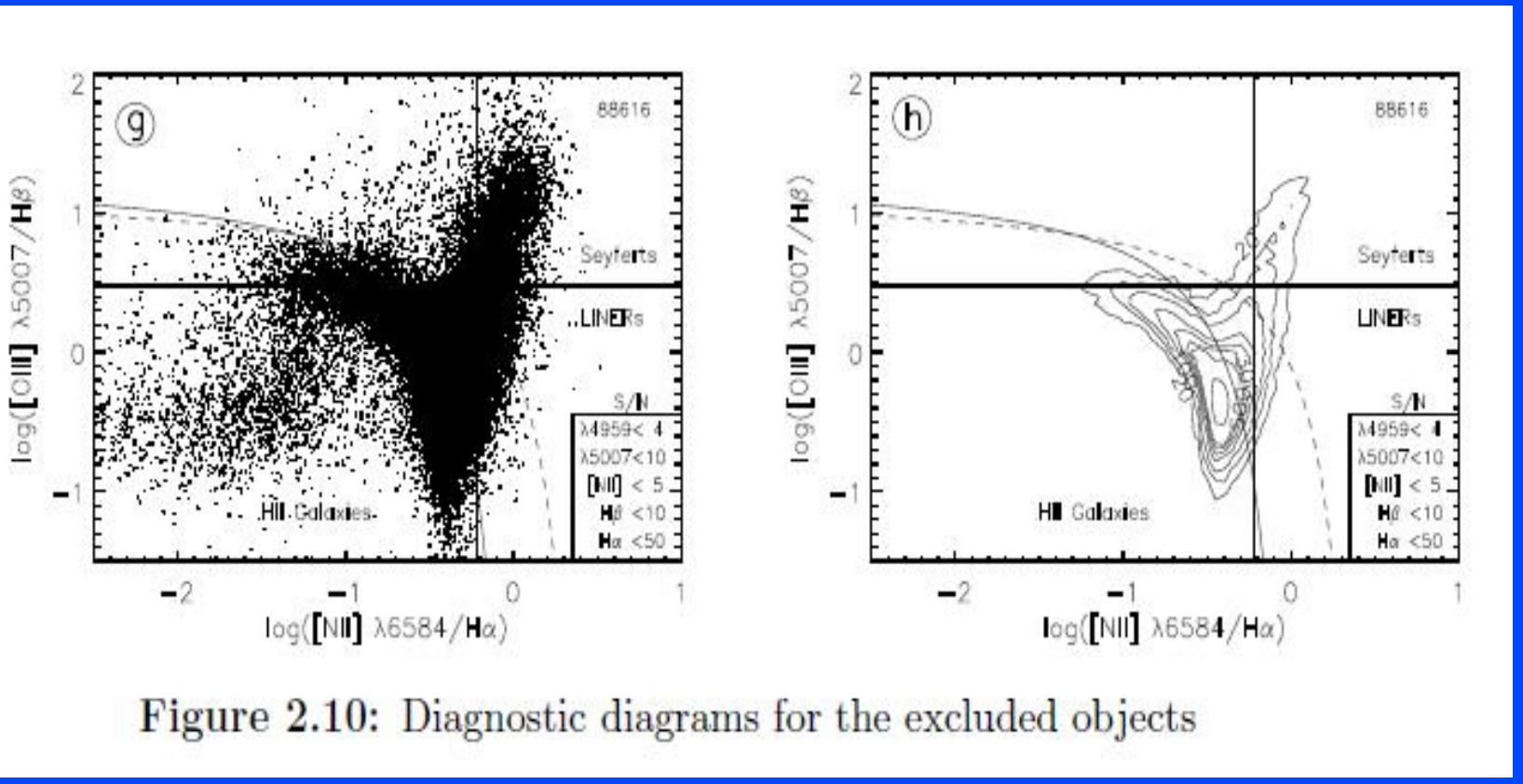



Figure 2.10: Diagnostic diagrams for the excluded objects

Objects outside the line width limits.

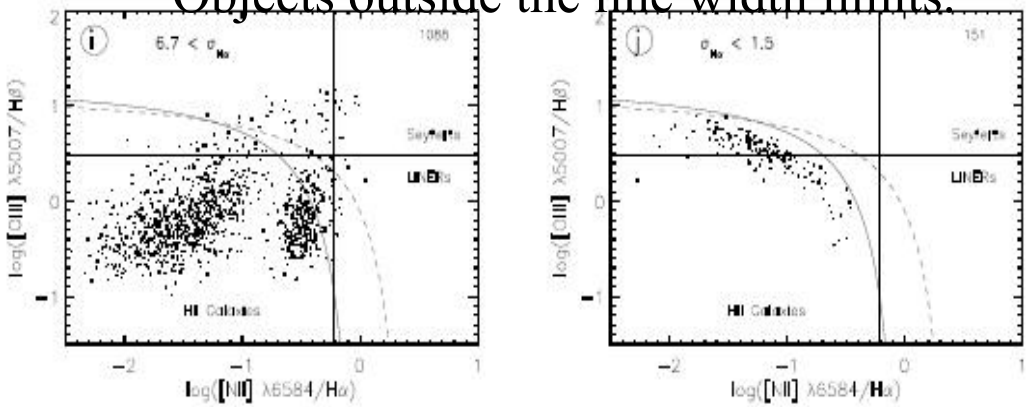



**Figure 2.13:** Objects below and above the $\sigma_{H\alpha}$ limits in figure 2.12

Final sample

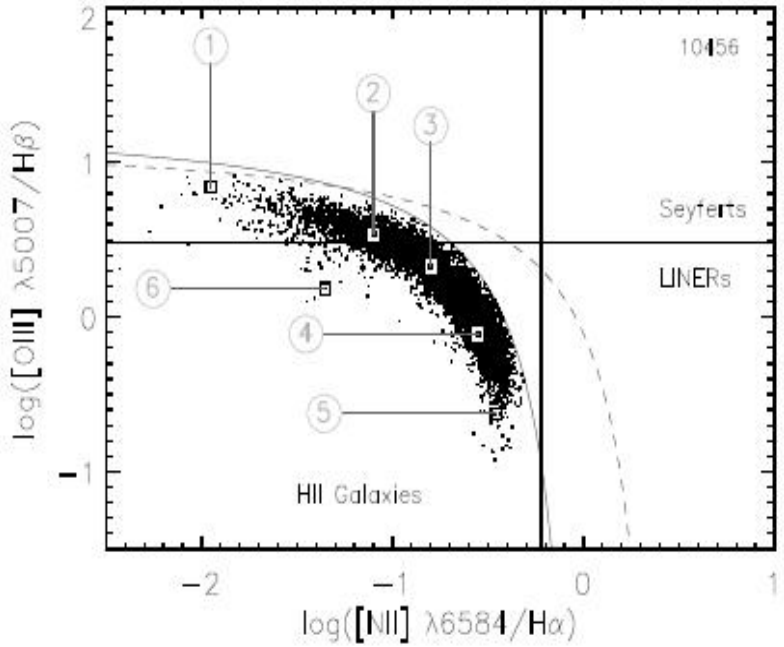



**Figure 2.14:** BPT diagram for the final sample. Squares indicate selected objects to show their spectra in plot 2.16.

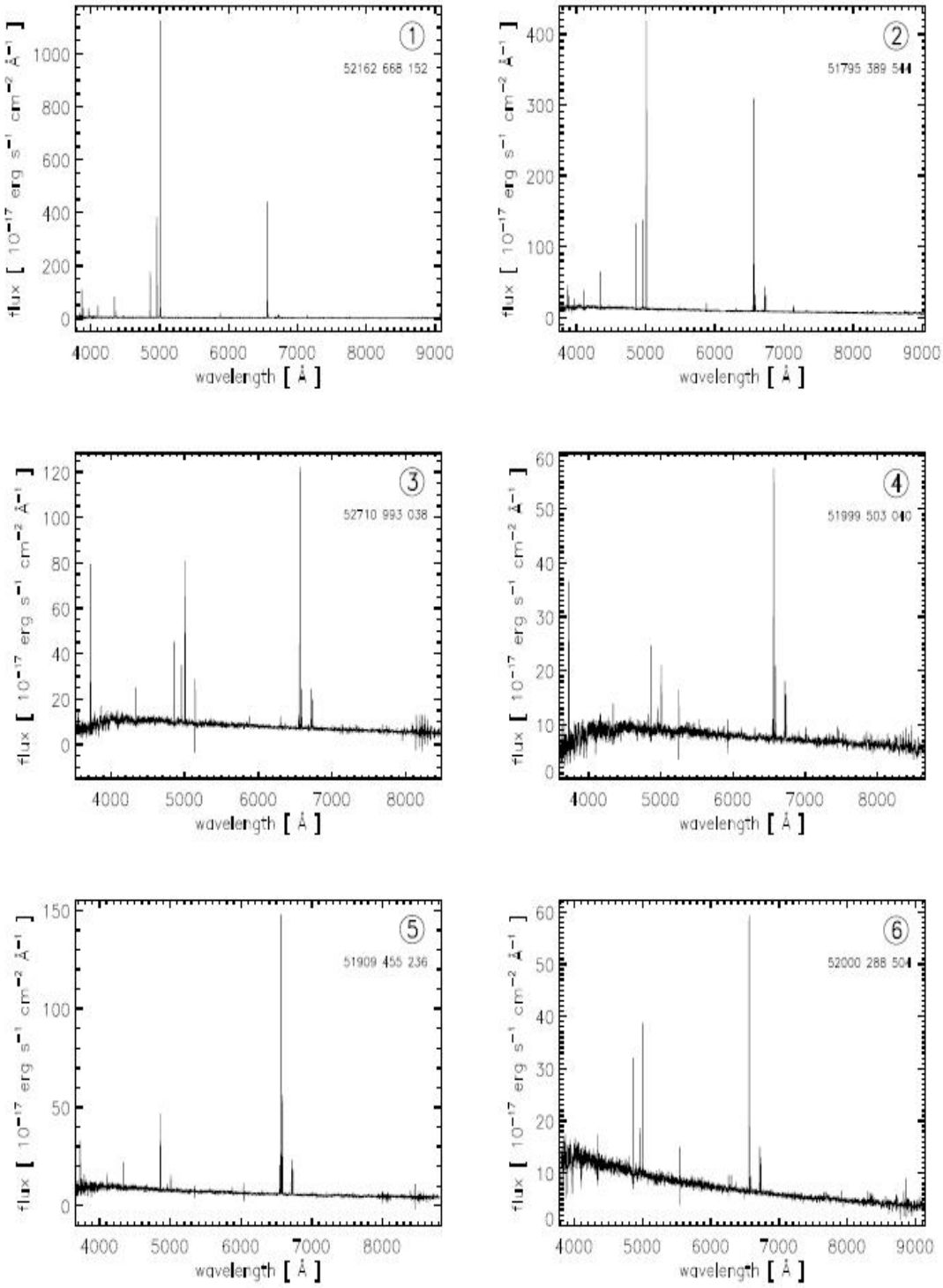



**Figure 2.16:** Spectra for the selected objects in figure 2.14.

# Final sample isocontours

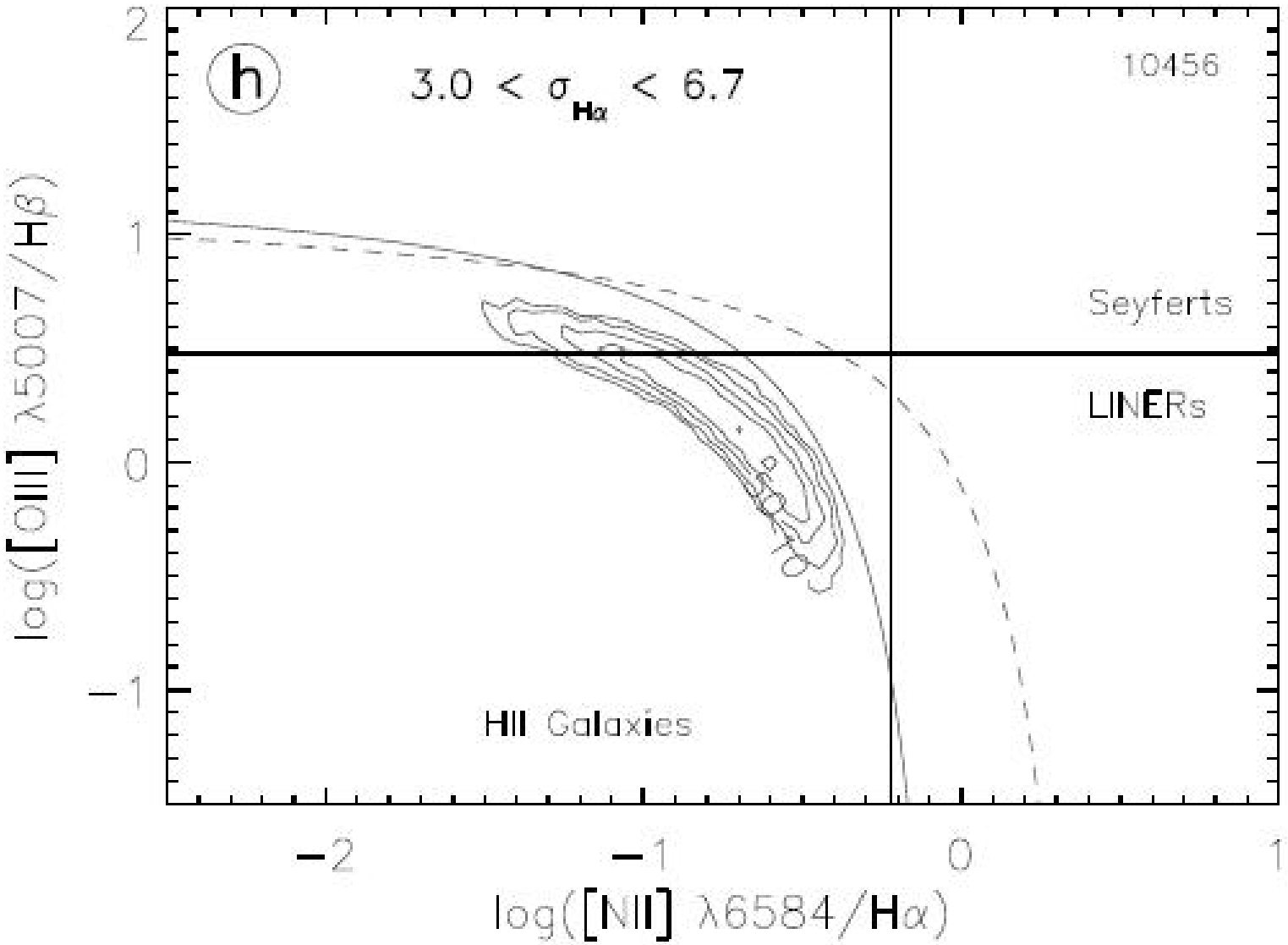



**Figure 2.15:** Isocontours for the BPT diagram for the final sample.

# Hα EW distribution

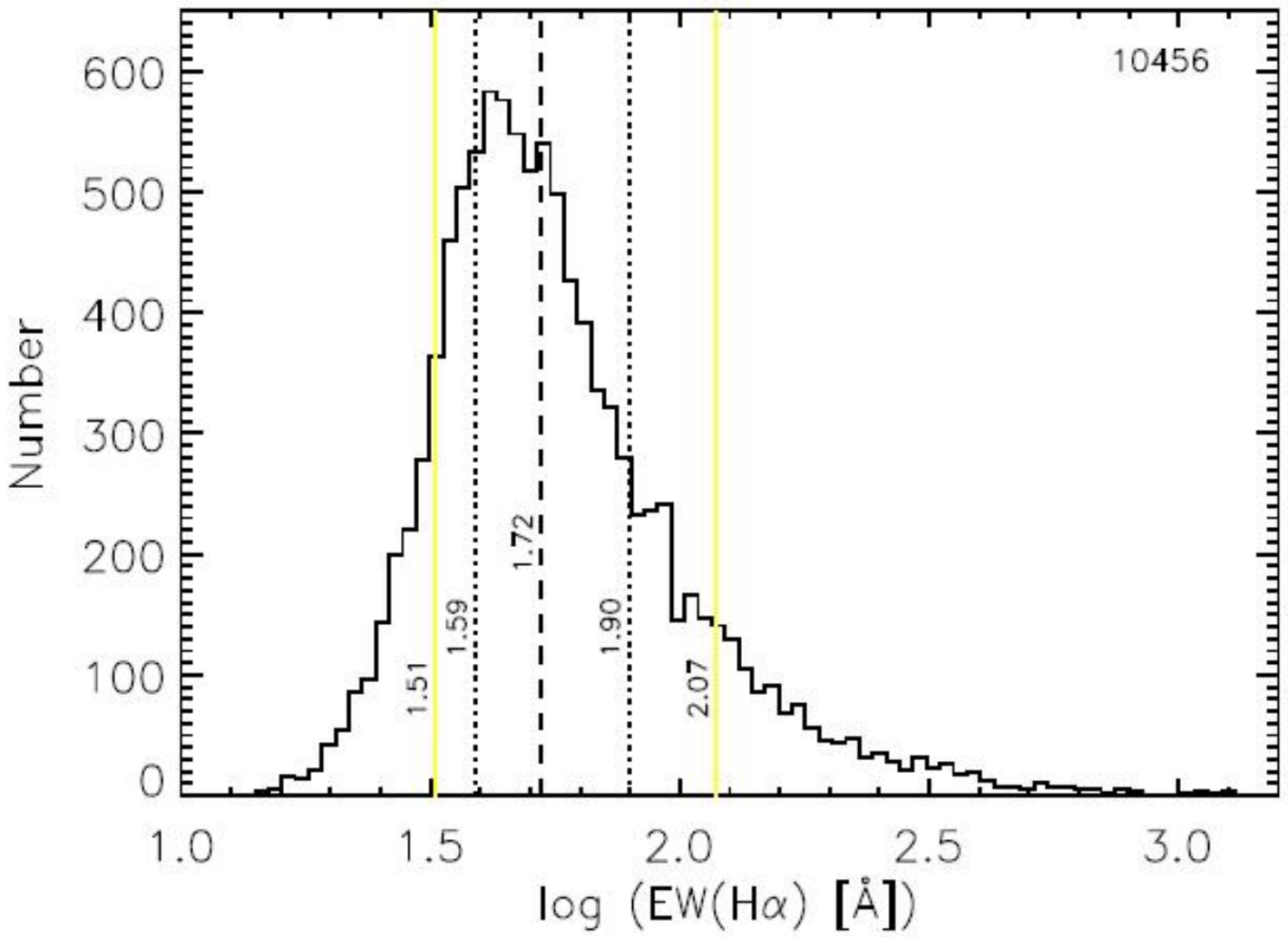



**Figure 3.1:** Distribution of EW(Hα). The dashed line indicates the median, dotted lines are for 25% and 75% of the distribution and grey lines are for 12.5% and 87.5% (first and last octiles).

# Hα EW vs time

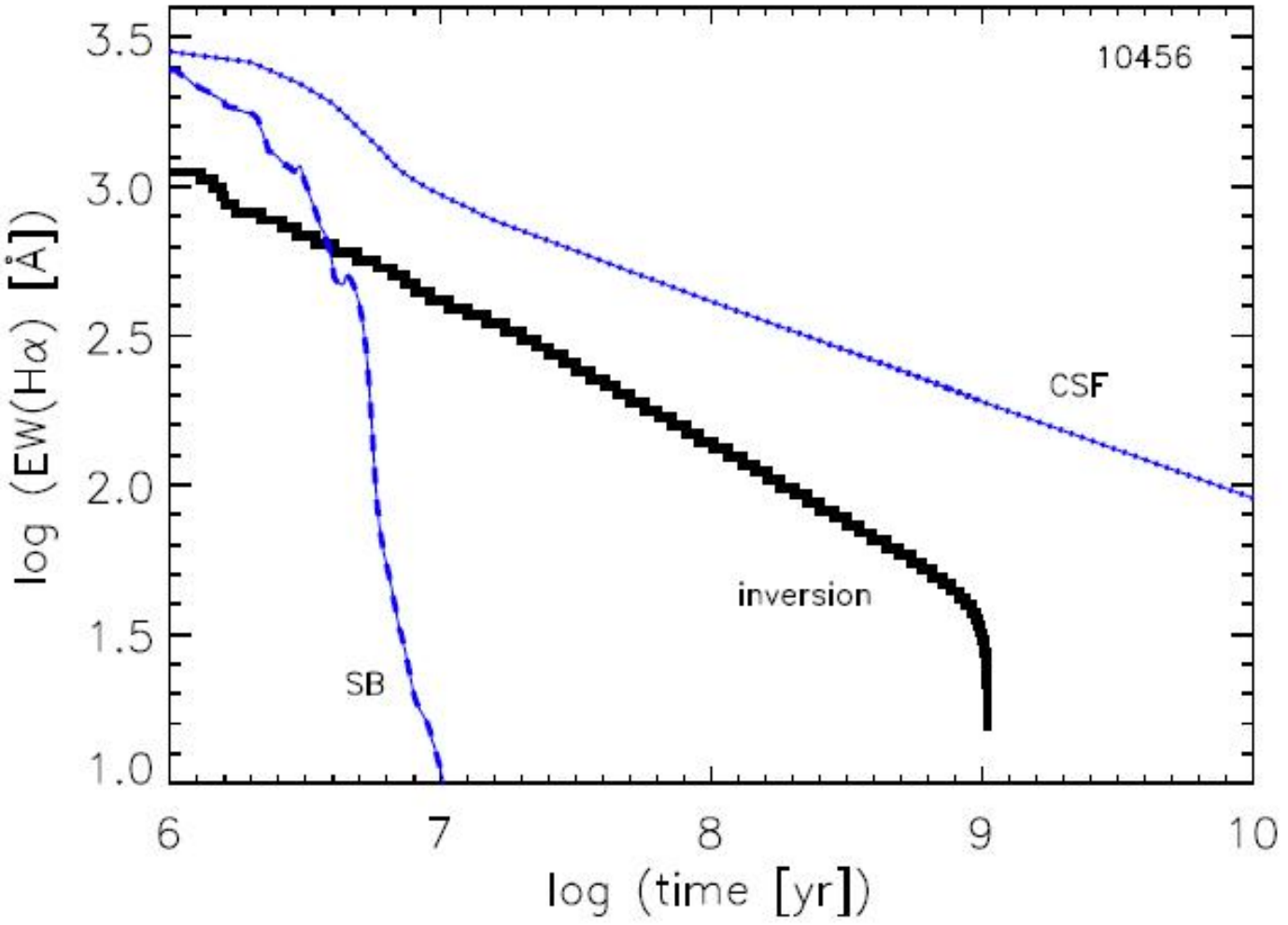



**Figure 3.3:** Recovered EW(Hα) distribution vs. log (time [yr]), obtained from the inversion procedure: corrected by underlying absorption (solid black line) and uncorrected (gray solid line). SB99 simulations results are included: CSF (dotted line) with $1M_{\odot}$ $yr^{-1}$ and SB (dashed line) with total mass equal to $10^6 M_{\odot}$.

# Optical continuum luminosity distribution

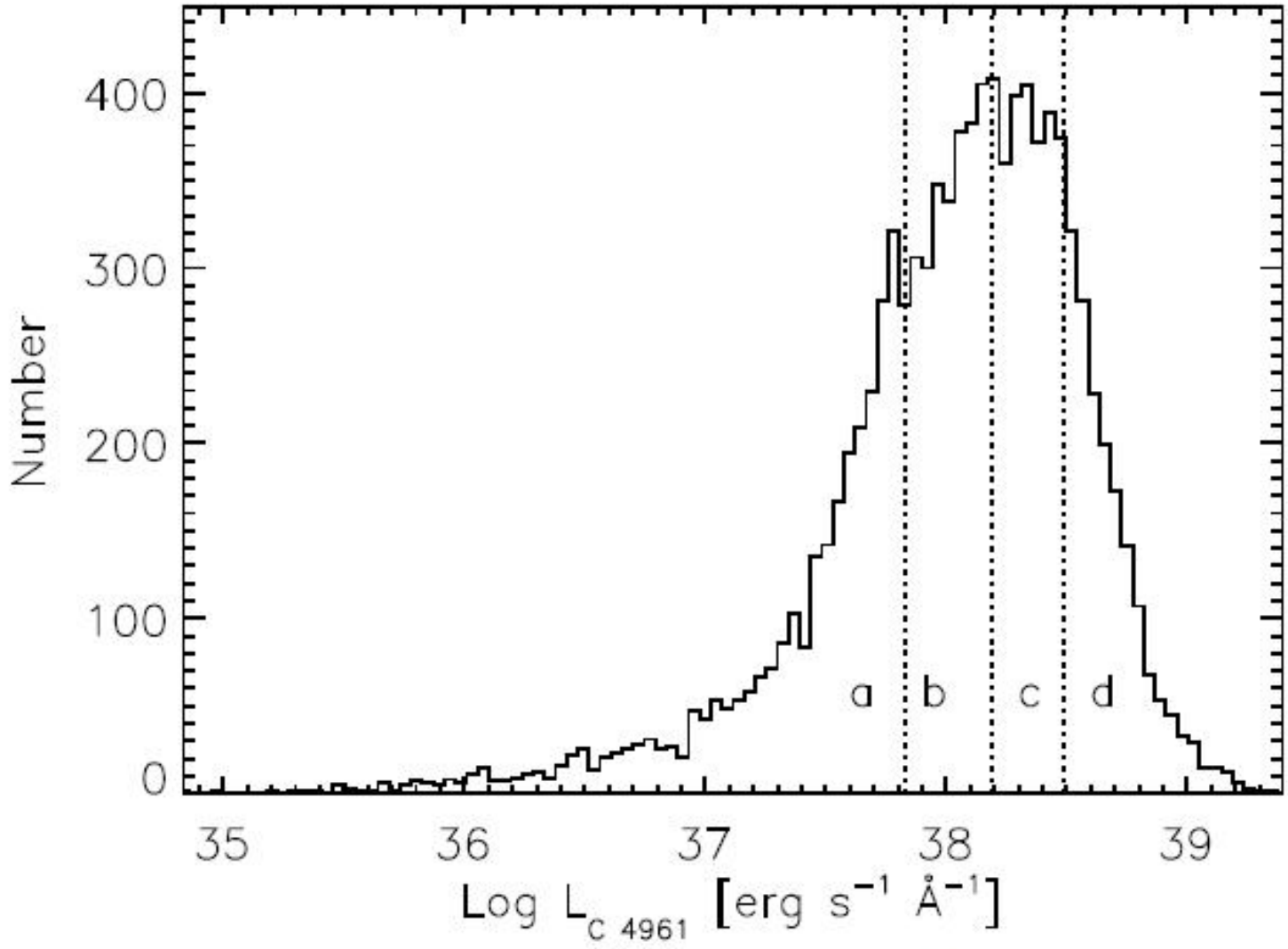



**Figure 3.6:** Log $L_{C4861}$ distribution for the sample. The dotted lines indicate the limits that divide the sample in quartiles.

# Optical continuum luminosity dependence

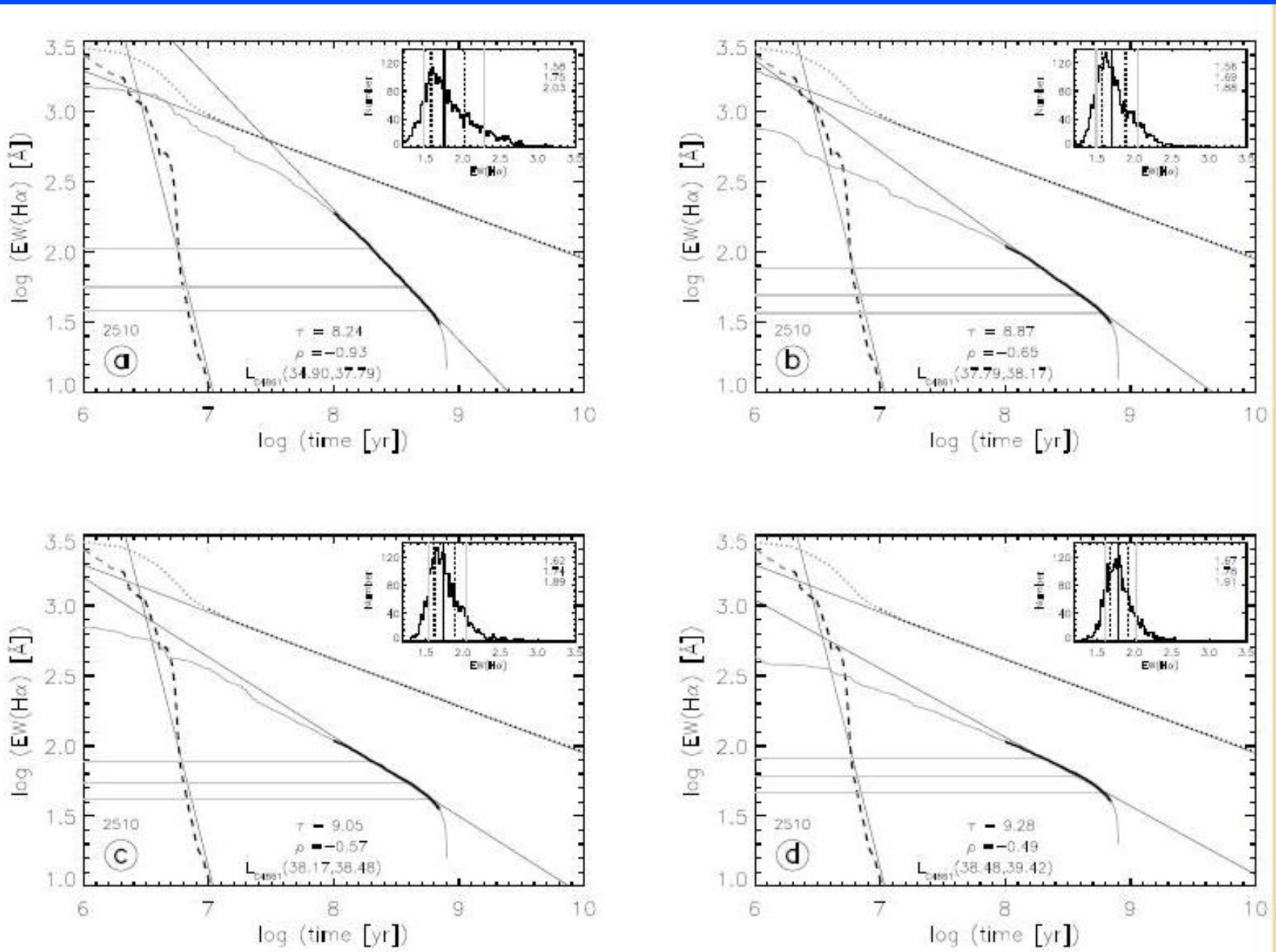



**Figure 3.7:** Inversion for the different subsamples with increasing $L_{C4861}$, letters correspond to the bins indicated in figure 3.6. The number of objects is above the letter. The insert in the upper right corner of each panel shows the EW(H$\alpha$) distribution used for the inversion.

# Models with decreasing SFR

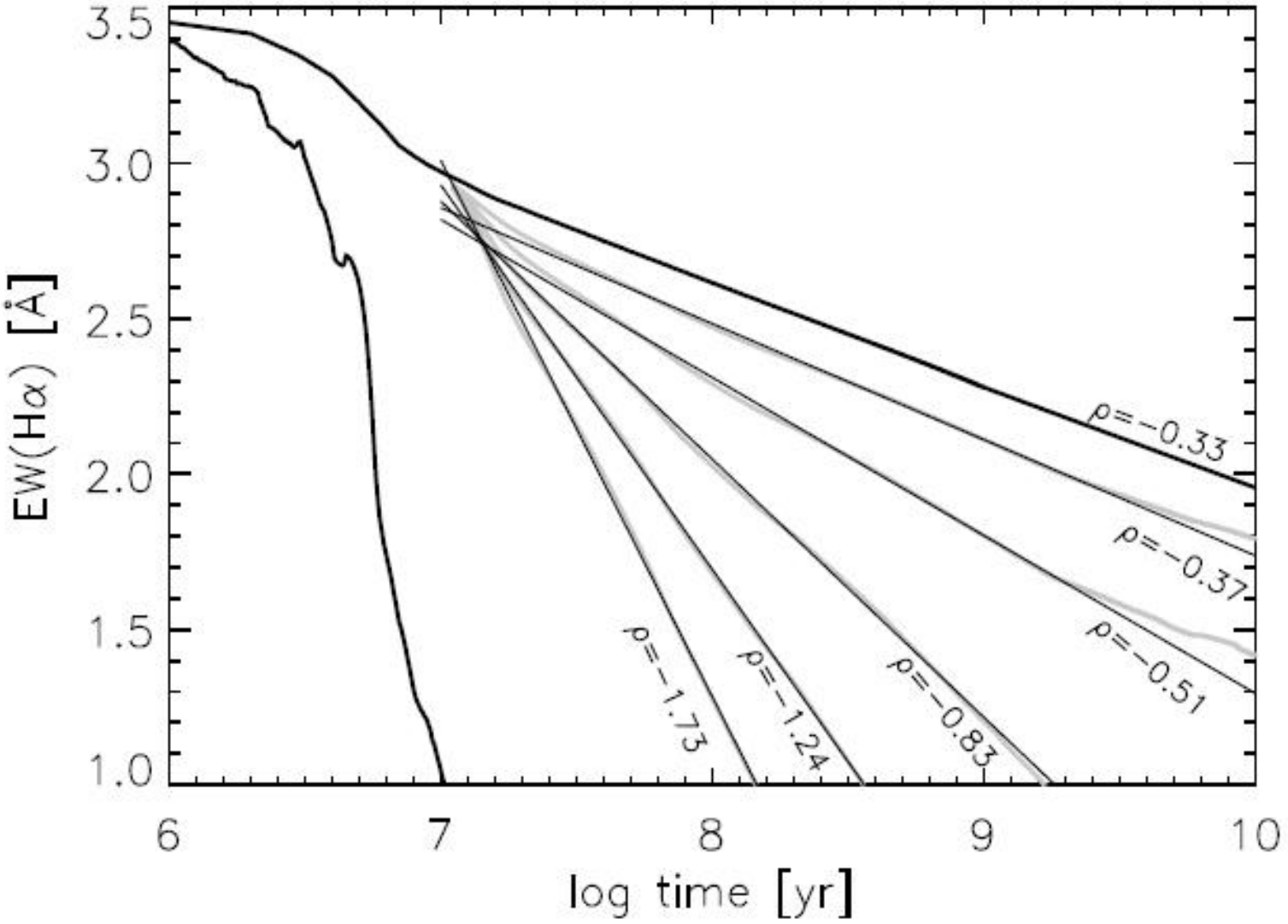



**Figure 3.4:** Models (kindly calculated by S. Silich) with decreasing star formation power law. The lines are for $SFR \propto t^{\mu}$ where $\mu$ is 0.0, -0.5, -1.0, -1.5, -2.0 and -2.5 starting from the CSF mode. $\rho$ is the slope for each line.

# Fits

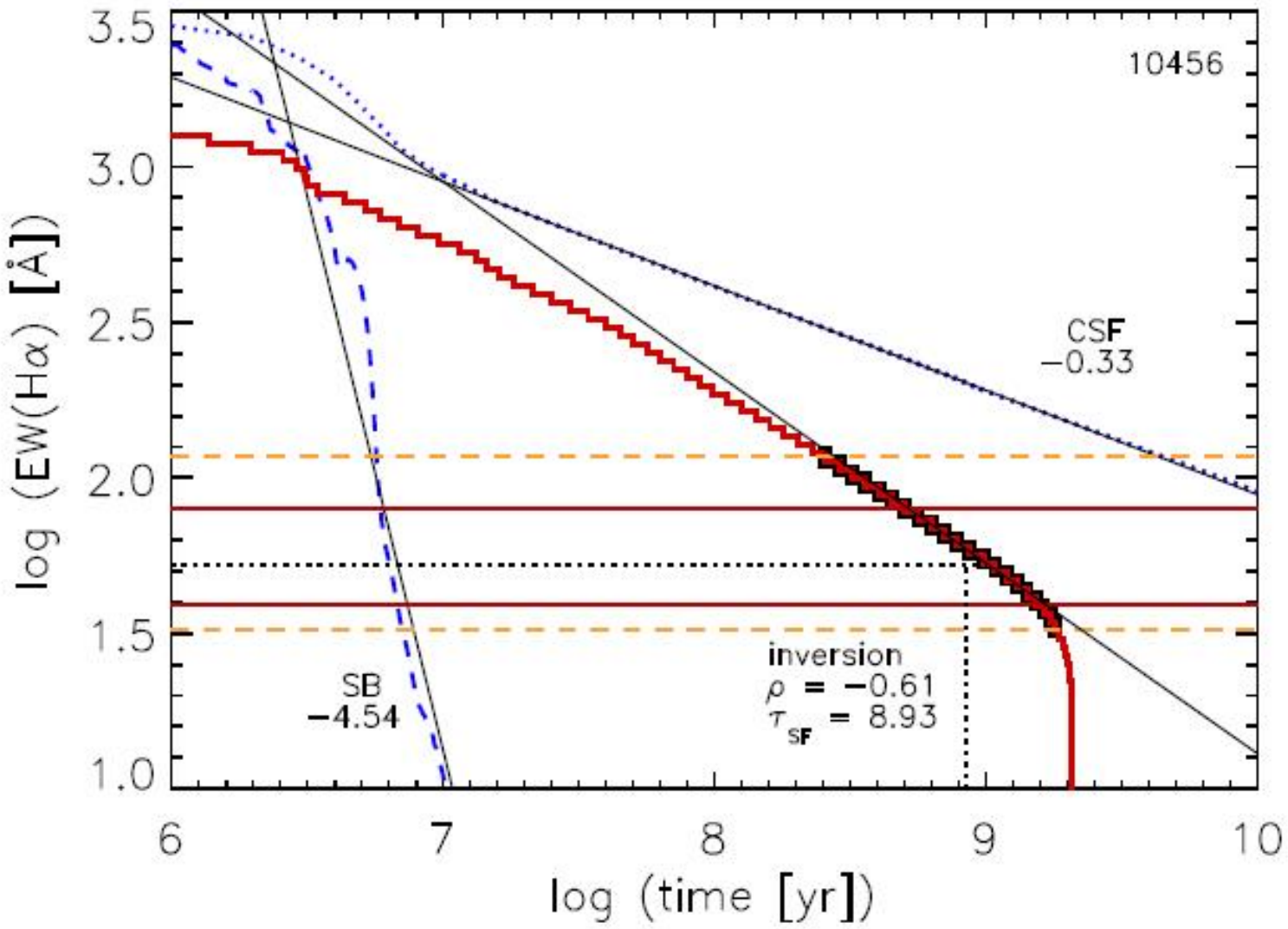



**Figure 3.5:** Log EW(H$\alpha$) vs log time. It shows the use of slopes to allocate time in the inversion from figure 3.3. The solid lines are approximations to the models and the inversion (excluding the first and last octiles), the number below each label is the associated slope. The timescale obtained is $\tau_{SF} = 8.93$

# Optical continuum Luminosity vs AGE

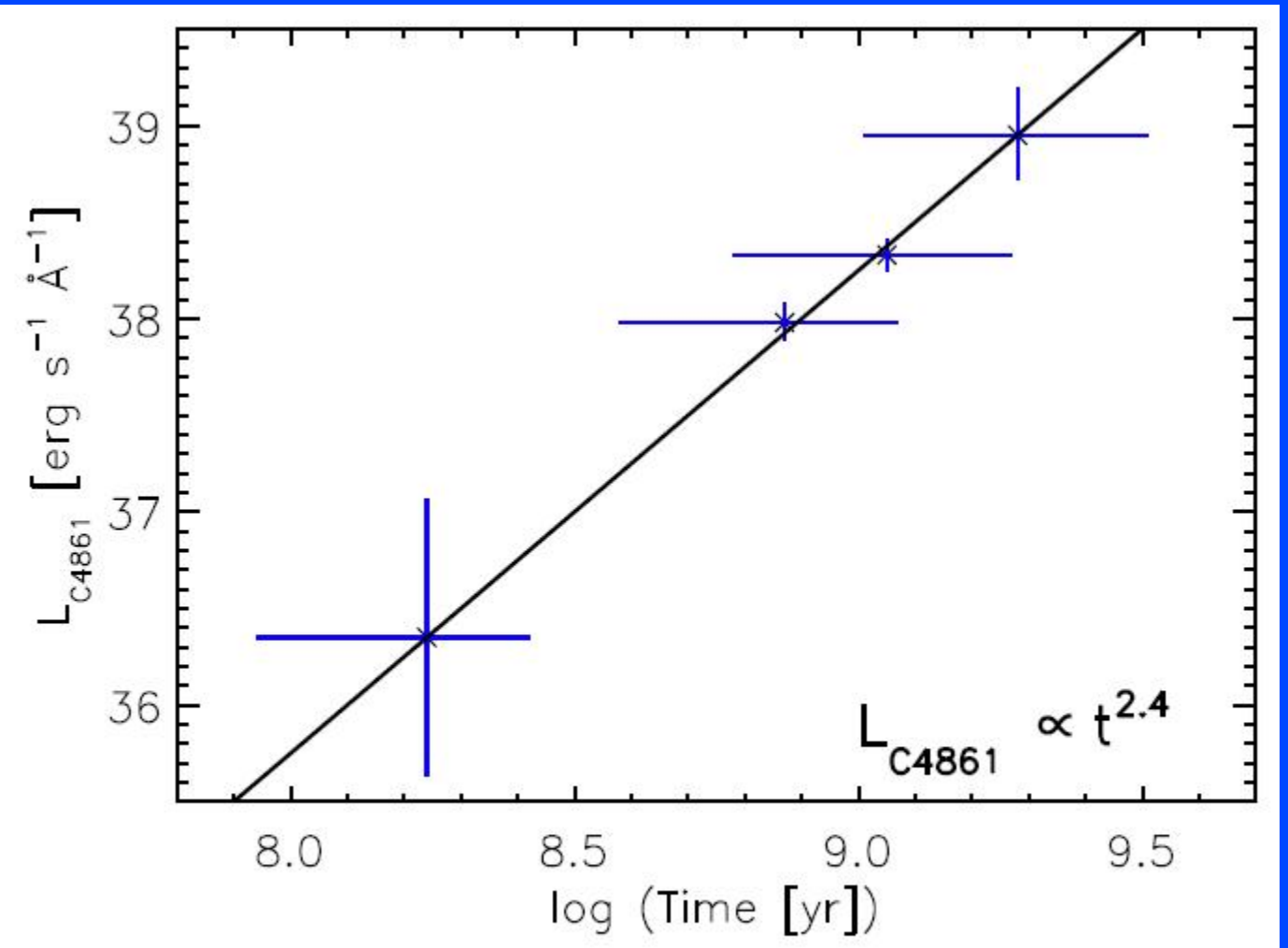



**Figure 3.8:** $L_{C4861}$ vs Time.

More luminous galaxies (starlight) are older

Nice fit!!

# Metallicity distribution

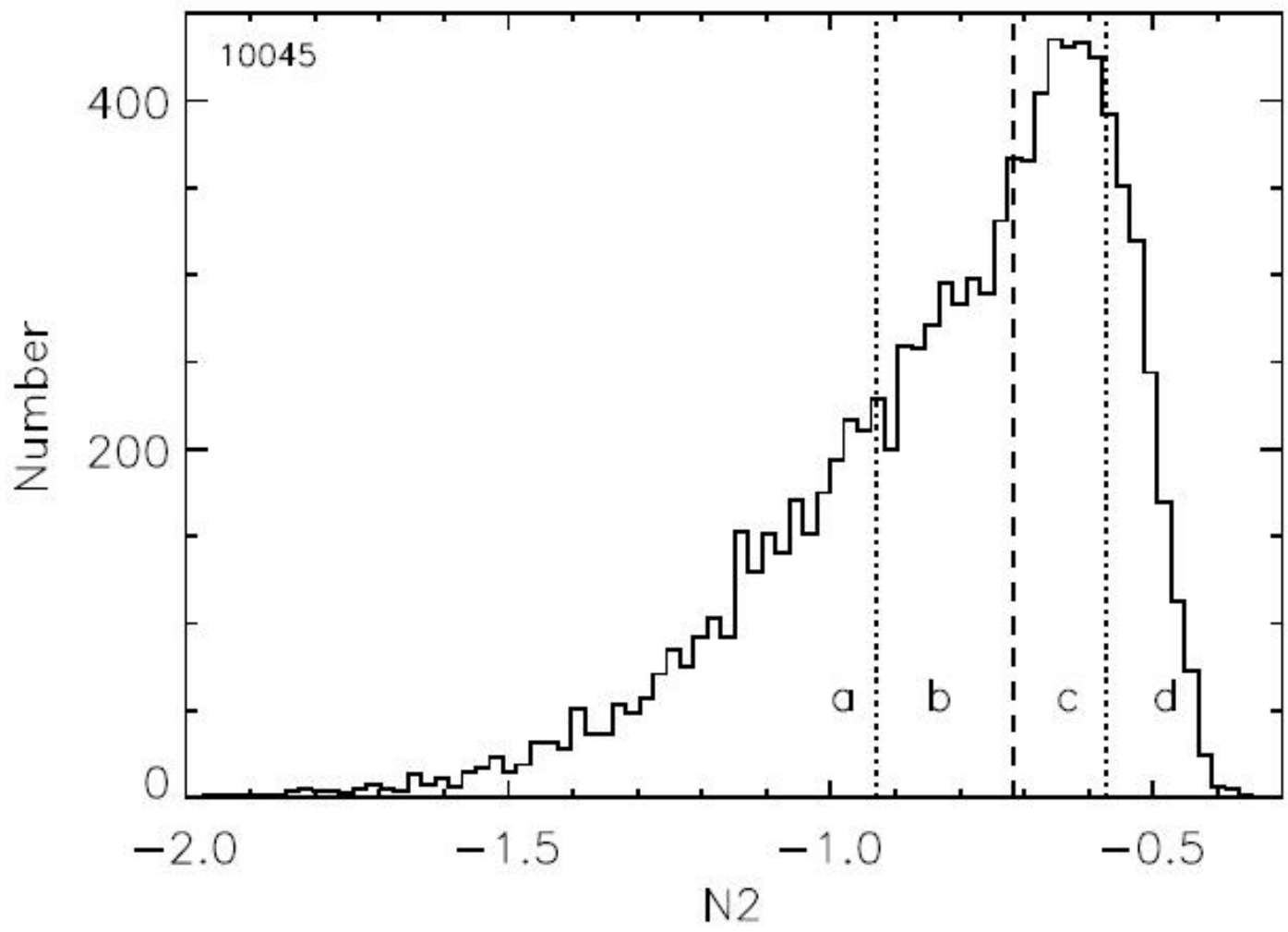



**Figure 3.14:** Distribution of galaxies from the sample over metallicity. N2 is used as indicator of the average ISM metallicity. Dashed line indicate the median and dotted lines the 25% and 75% of the distribution

# Metallicity dependence

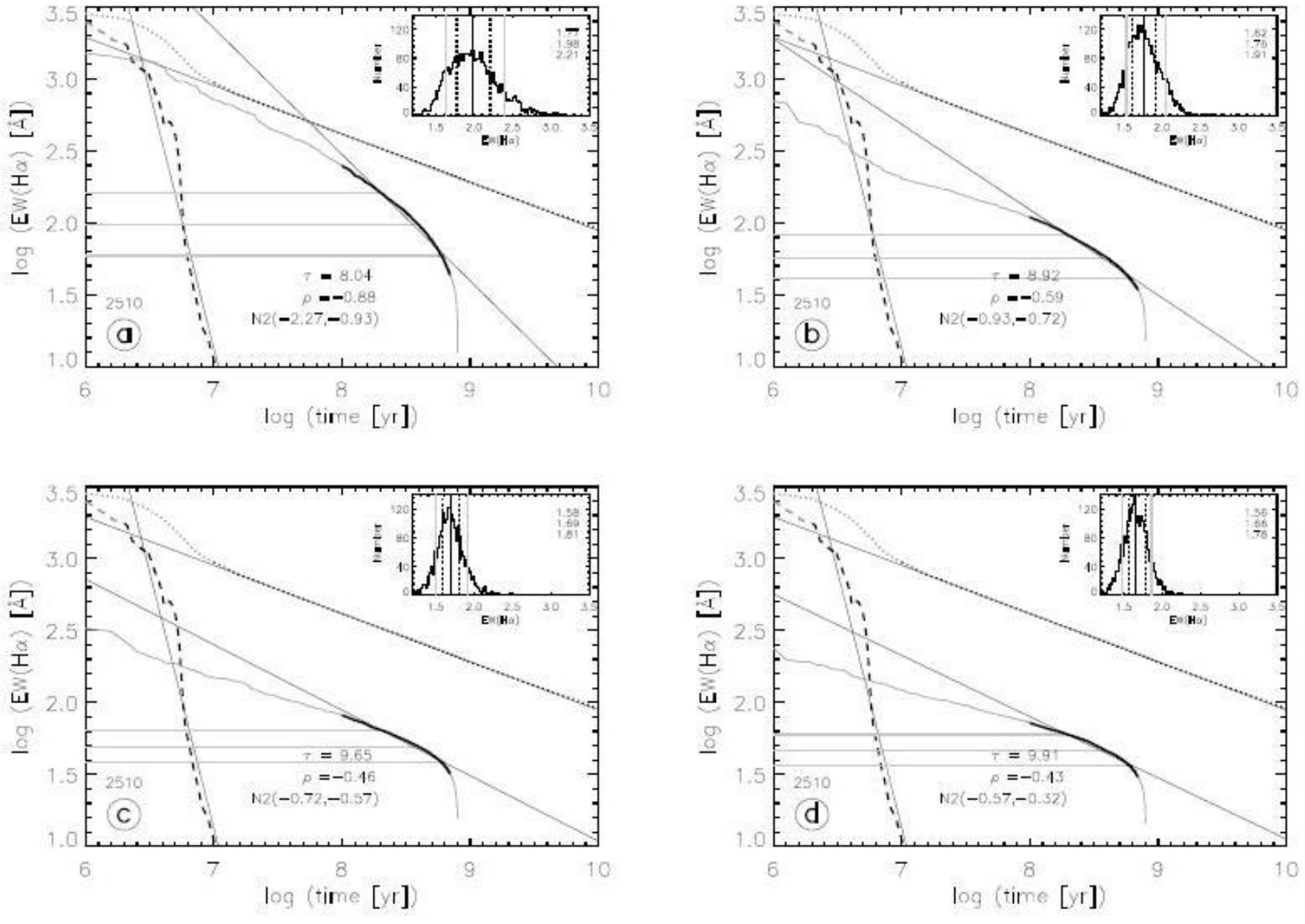



**Figure 3.15:** Inversion for data subsets of increasing metallicity (N2). The letters correspond to the bins in figure 3.14

# Metal content vs AGE

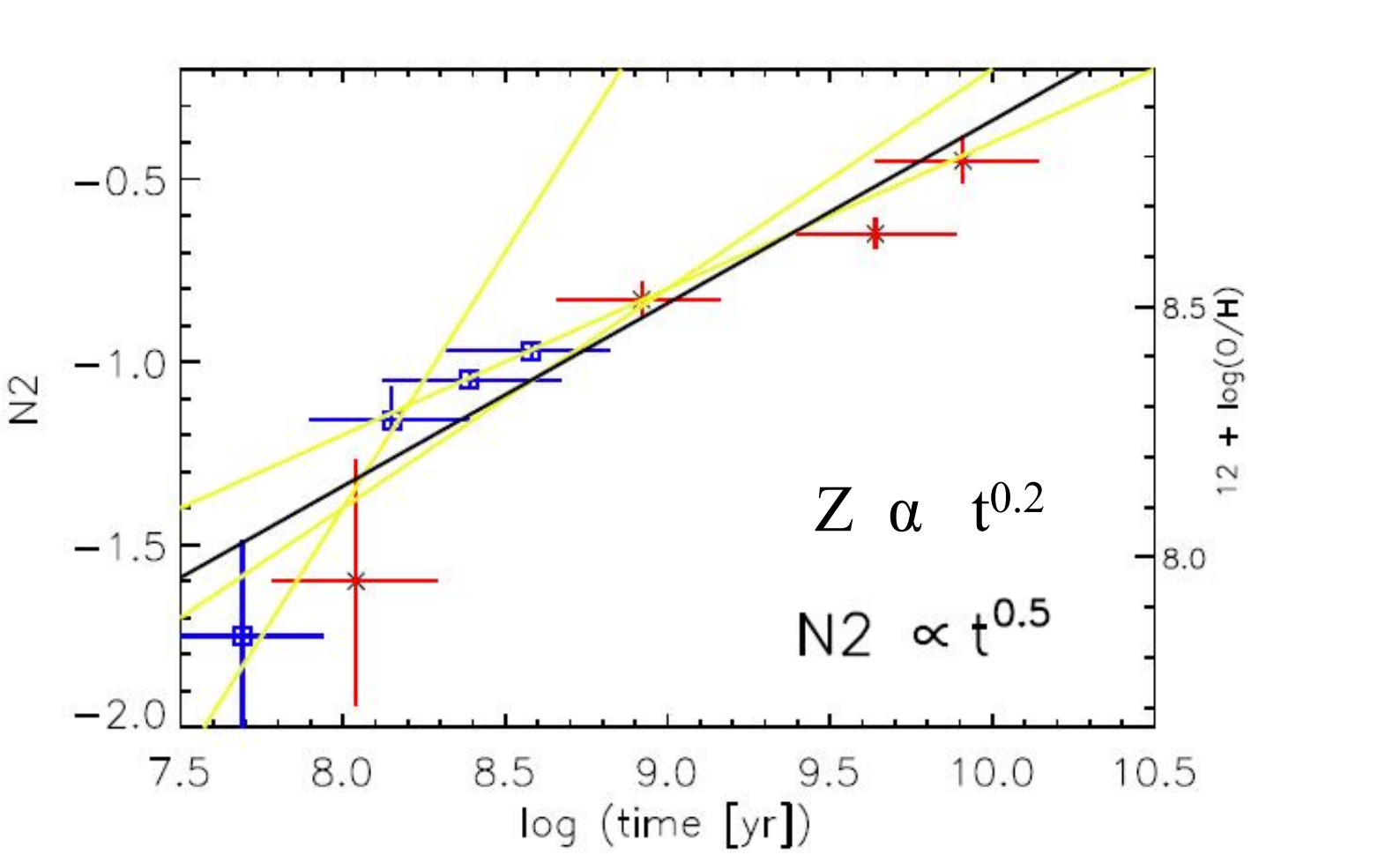



**Figure 3.25:** N2 and metallicity against time as obtained from different subsamples in figures 3.15 and 3.18. Bars are the range of values around the median (central 50% of the distribution).

Metal rich galaxies are older

# Distribution of IR luminosity (Z')

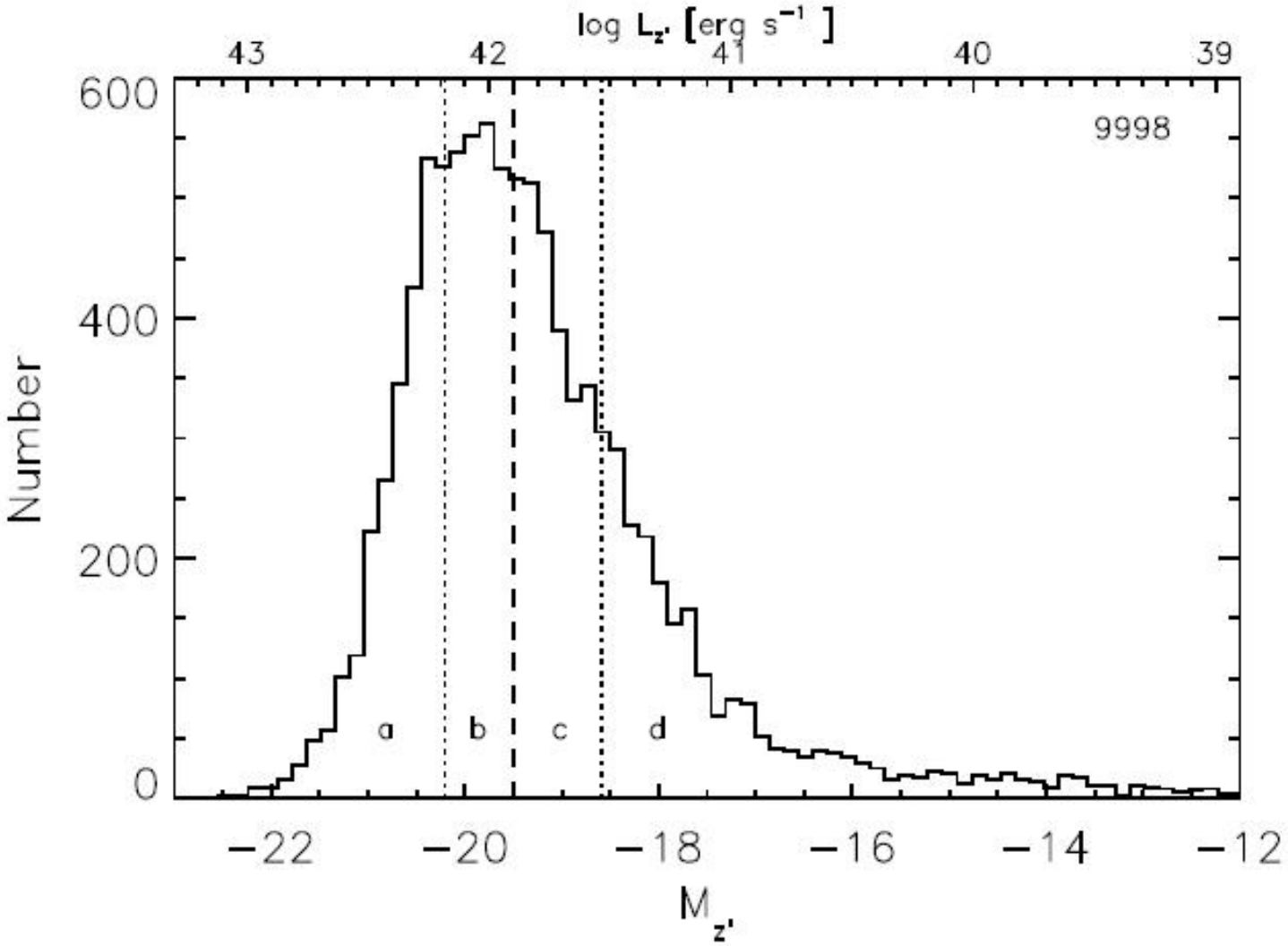



**Figure 4.9:** Distribution of absolute magnitude, the upper scale shows the luminosity

# Mass estimate from IR luminosity and concentration parameter

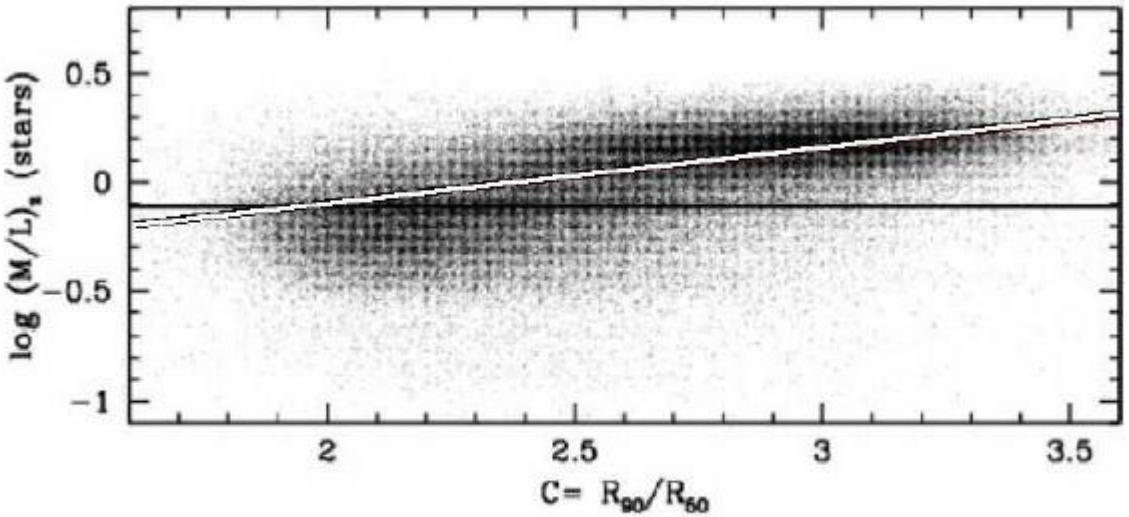



**Figure 4.10:** Log (M/L) in solar units as function of the concentration parameter (figure 13 from Kauffmann et al. (2003)). The line is the fit used to calculate the masses.

# Mass distribution

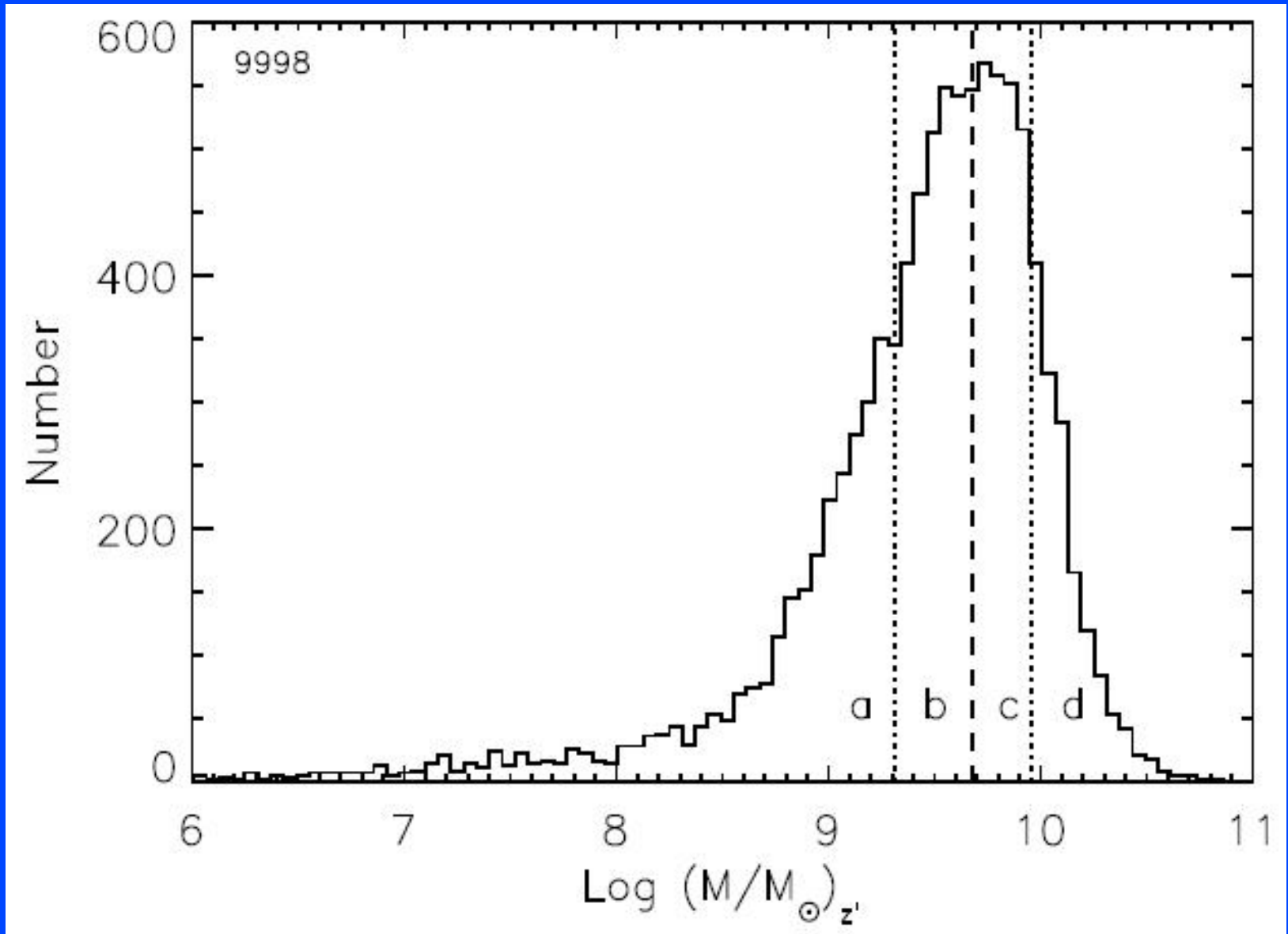



**Figure 4.12:** Mass distribution in solar units.

# Mass dependence

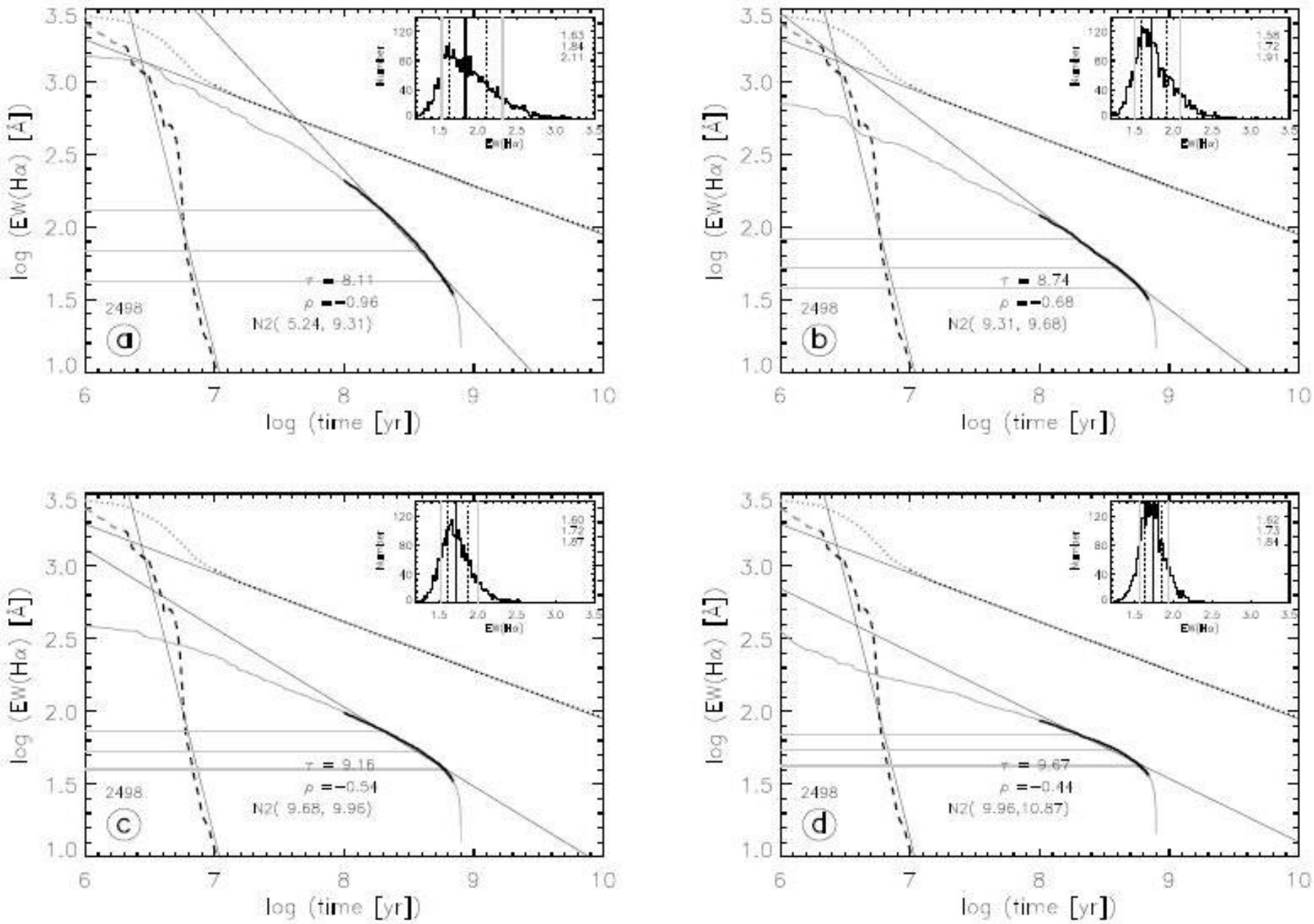



**Figure 4.13:** Inversion for data subsets of increasing mass. The letters correspond to the bins in figure 4.12.

# Stellar mass vs AGE

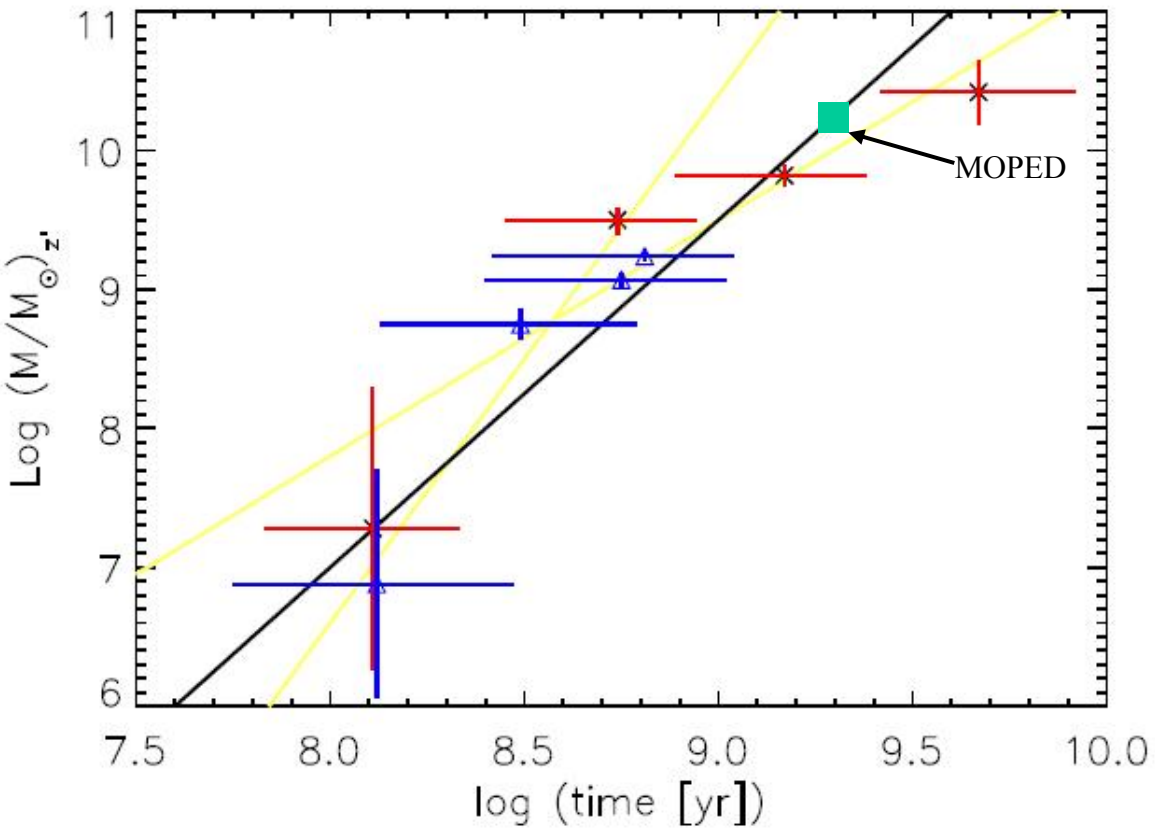



**Figure 4.16:** Mass as a function of time as obtained from the inversion over divisions in figure 4.12 (black symbols) and in figure 4.14 (grey symbols). The black line represents a time dependence on the mass of the form $\sim M \propto t^{2.5}$. Bars are the range of values around the median (centra 50 % of the distribution).

Massive galaxies are older.

Low mass galaxies are younger

# Continuity with higher masses

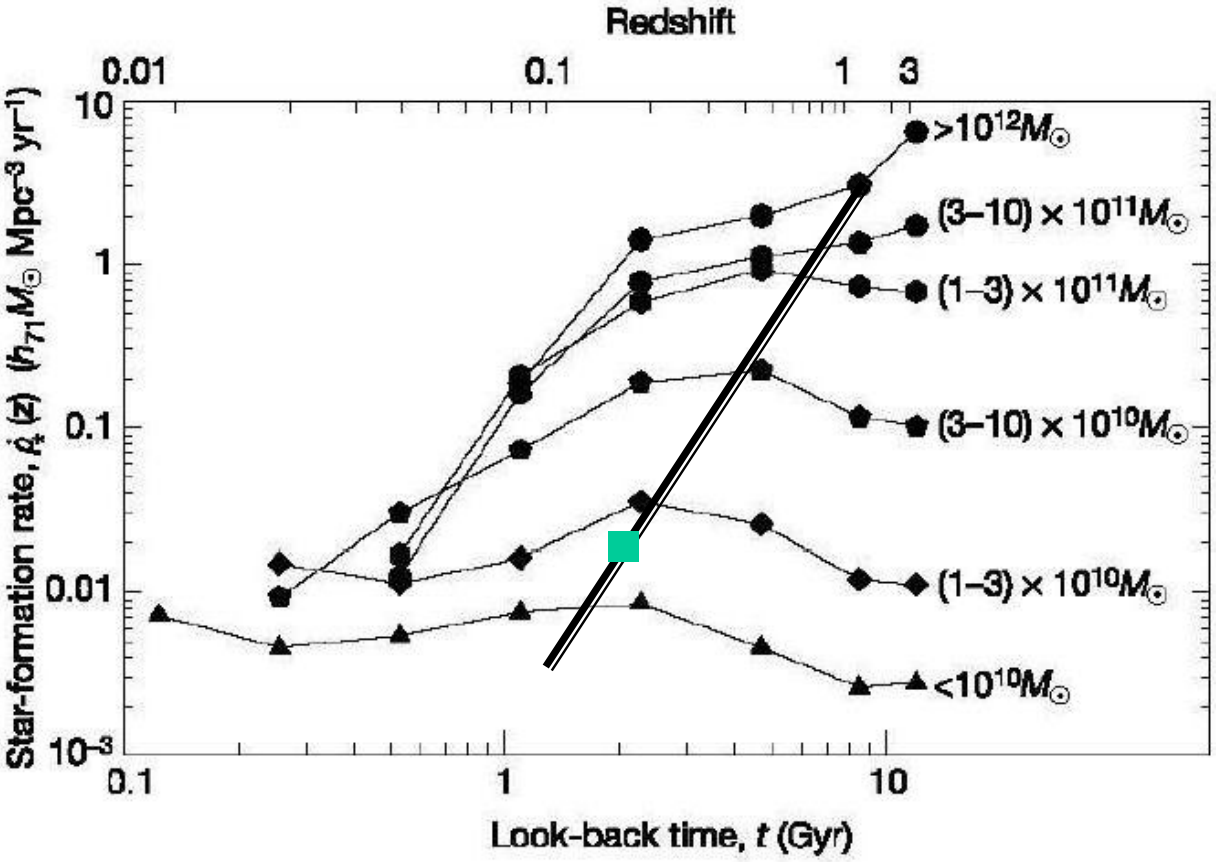



Figure 4.18: SFR vs. lookback time as a function of the galaxy mass (from (Heavens et al., 2004)).

# Conclusions

The Madau-Lilly diagram is an average over galaxy mass

Galaxy formation seems to follow different paths according to the total galaxy mass.

Our analysis indicates that even among the lowest mass starforming galaxies:

- The most massive galaxies formed their stars in a short time long time ago.
- The lowest mass galaxies are still forming stars

The results support downsizing even down to the lowest mass galaxies known.

Therefore if there is a single mechanism responsible for downsizing over the whole galaxian mass range from giant ellipticals down to low mass starforming dwarfs, quenching of starformation by AGN activity cannot be the main mechanism behind downsizing.

# Metallicity vs AGE for all HII galaxies

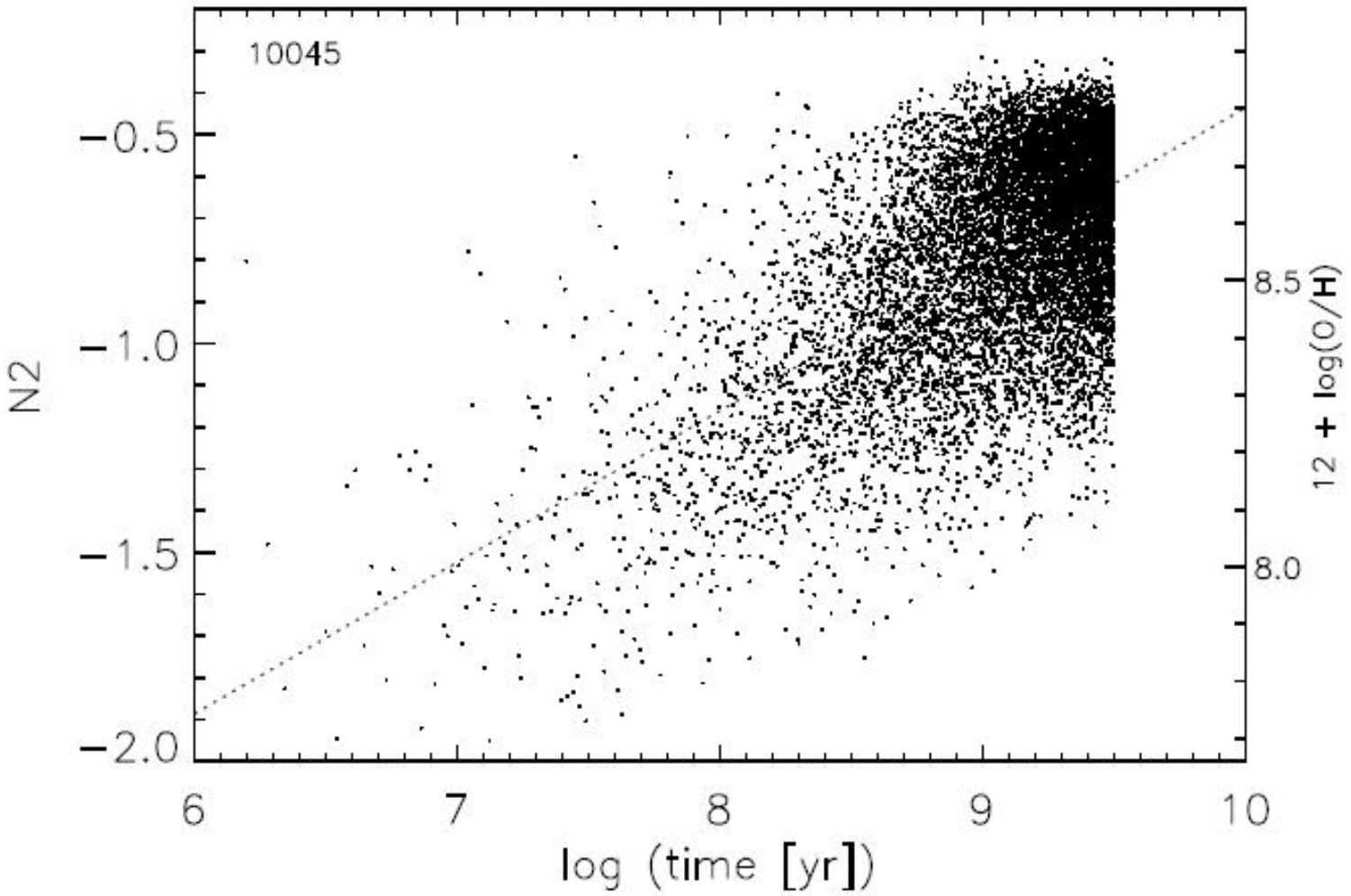



**Figure 3.21:** The metallicity indicator N2 as a function of time. The time is obtained from the whole sample inversion.

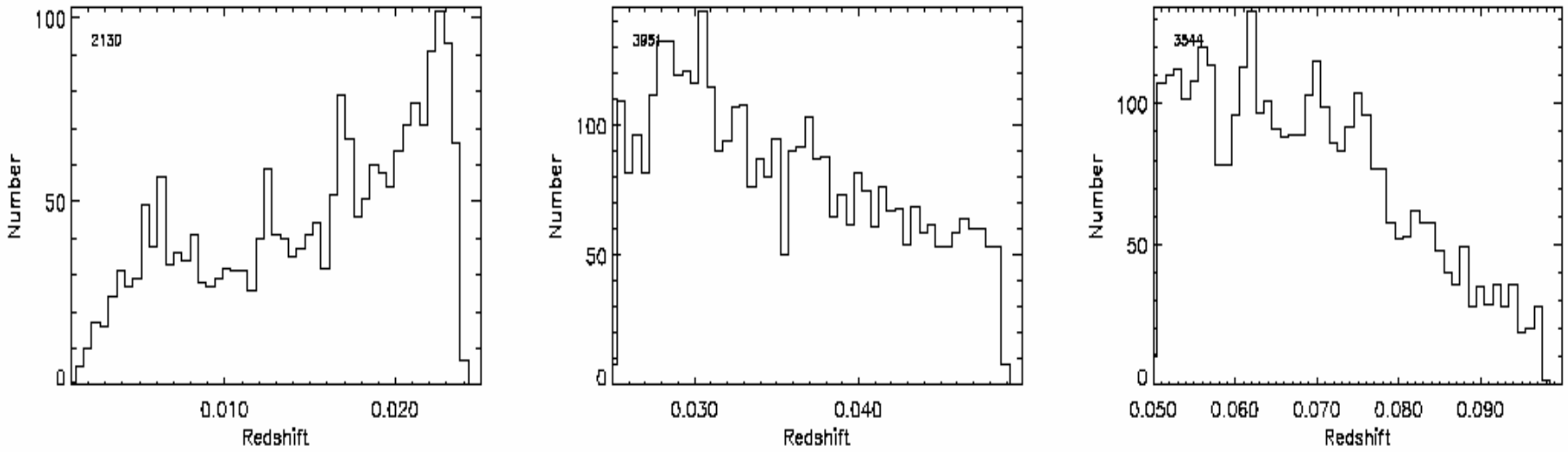
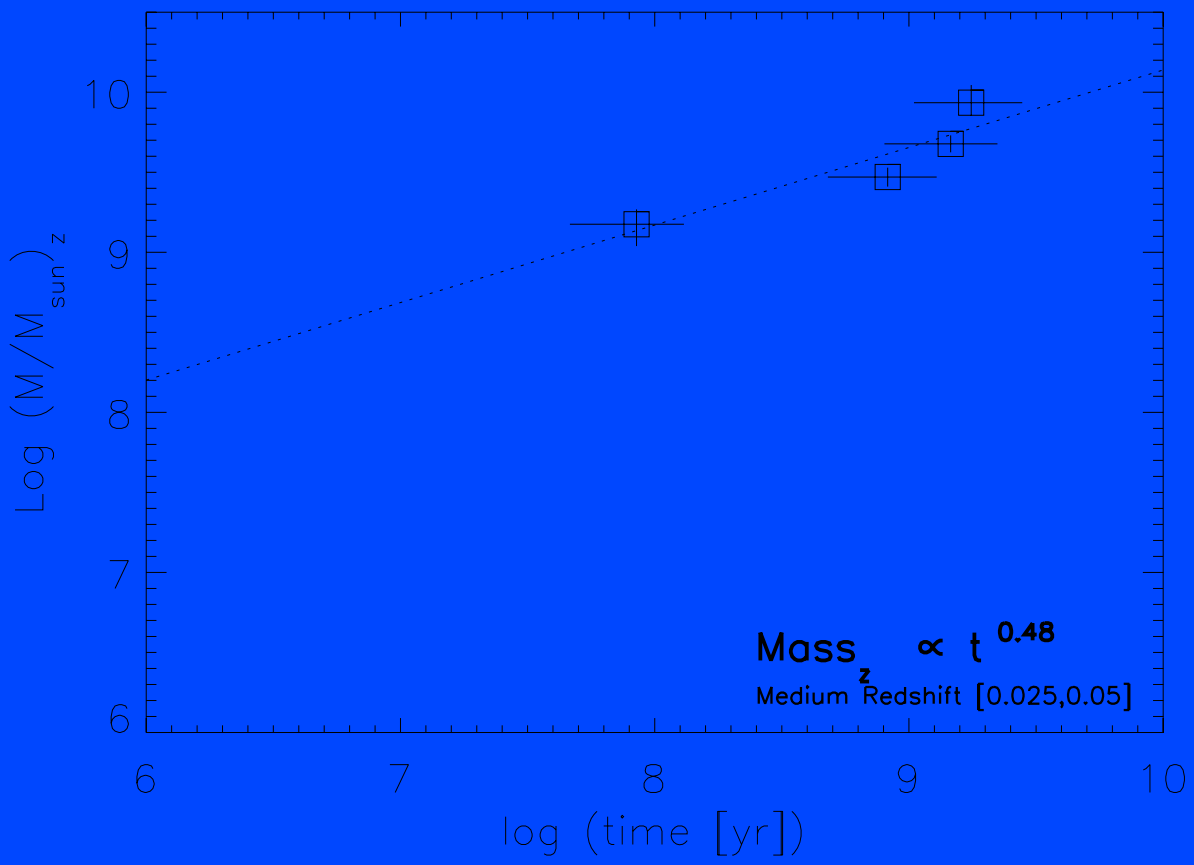
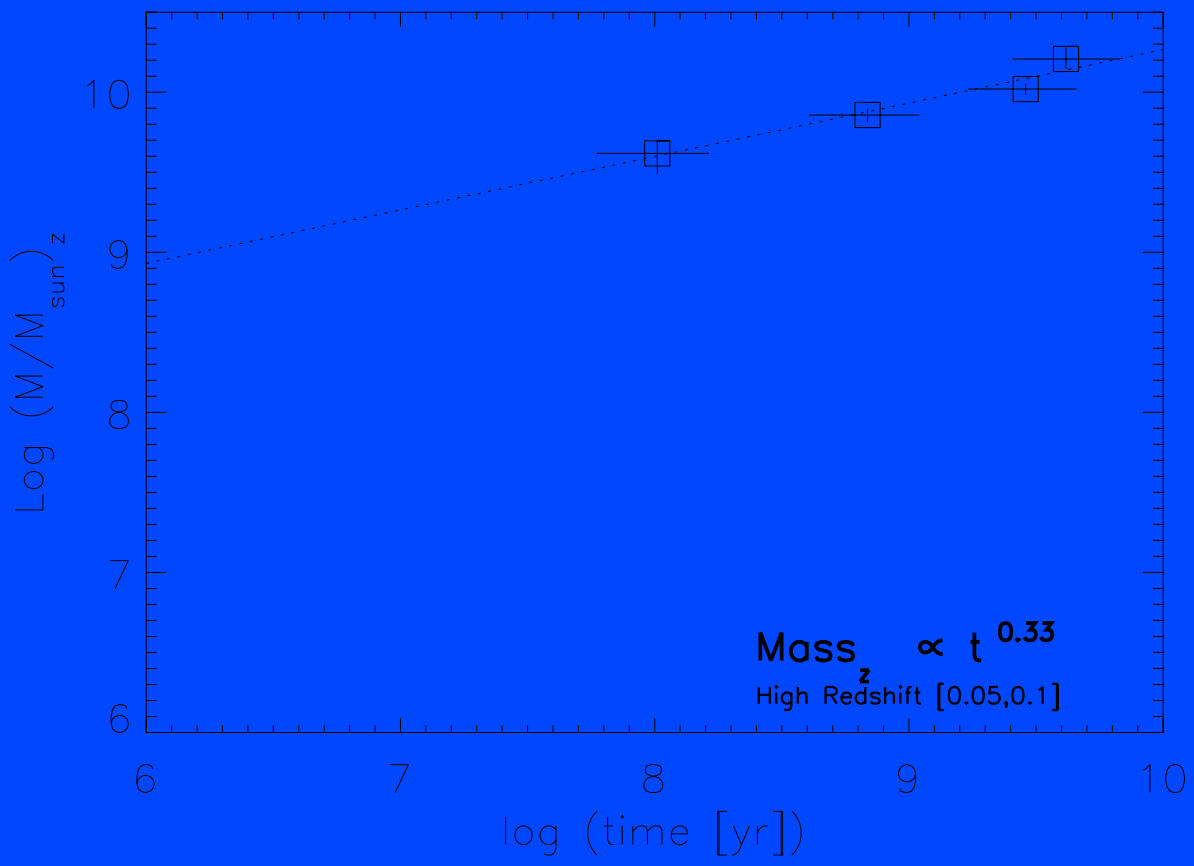
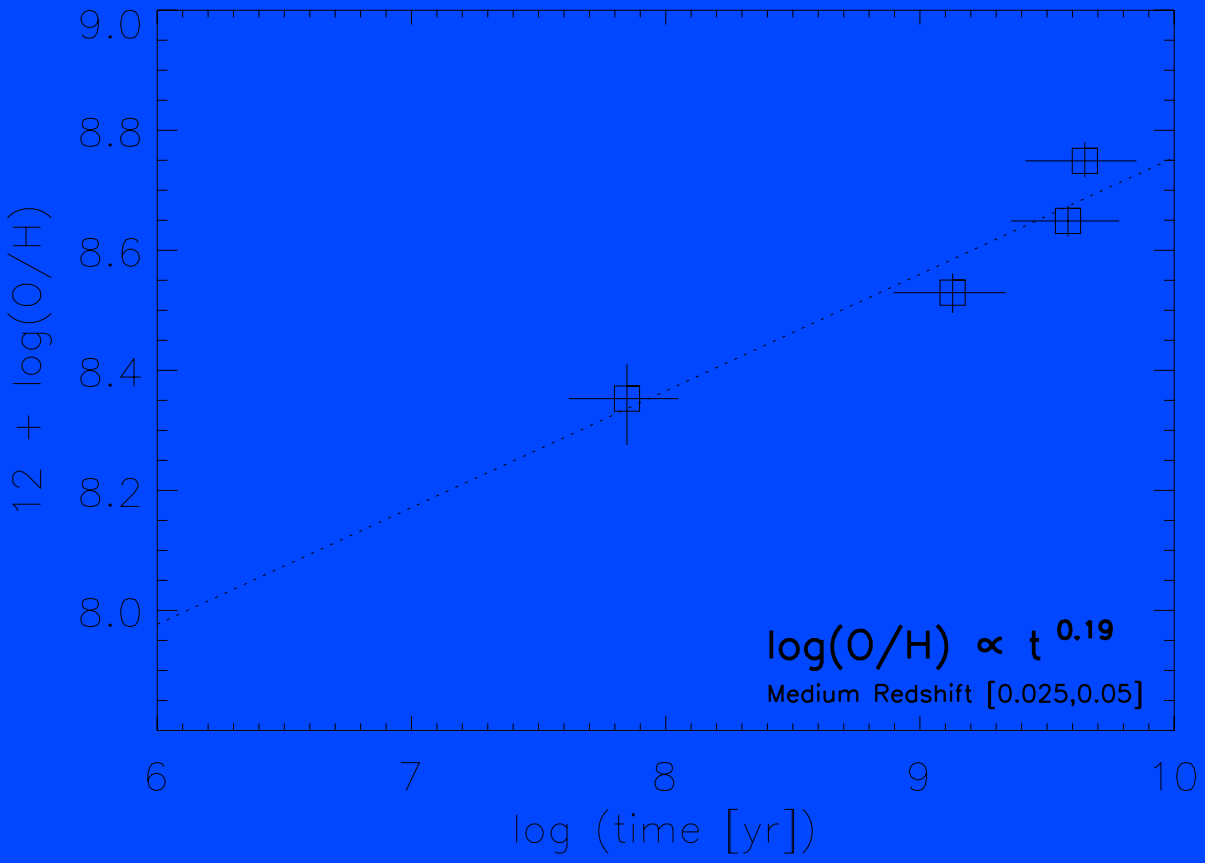
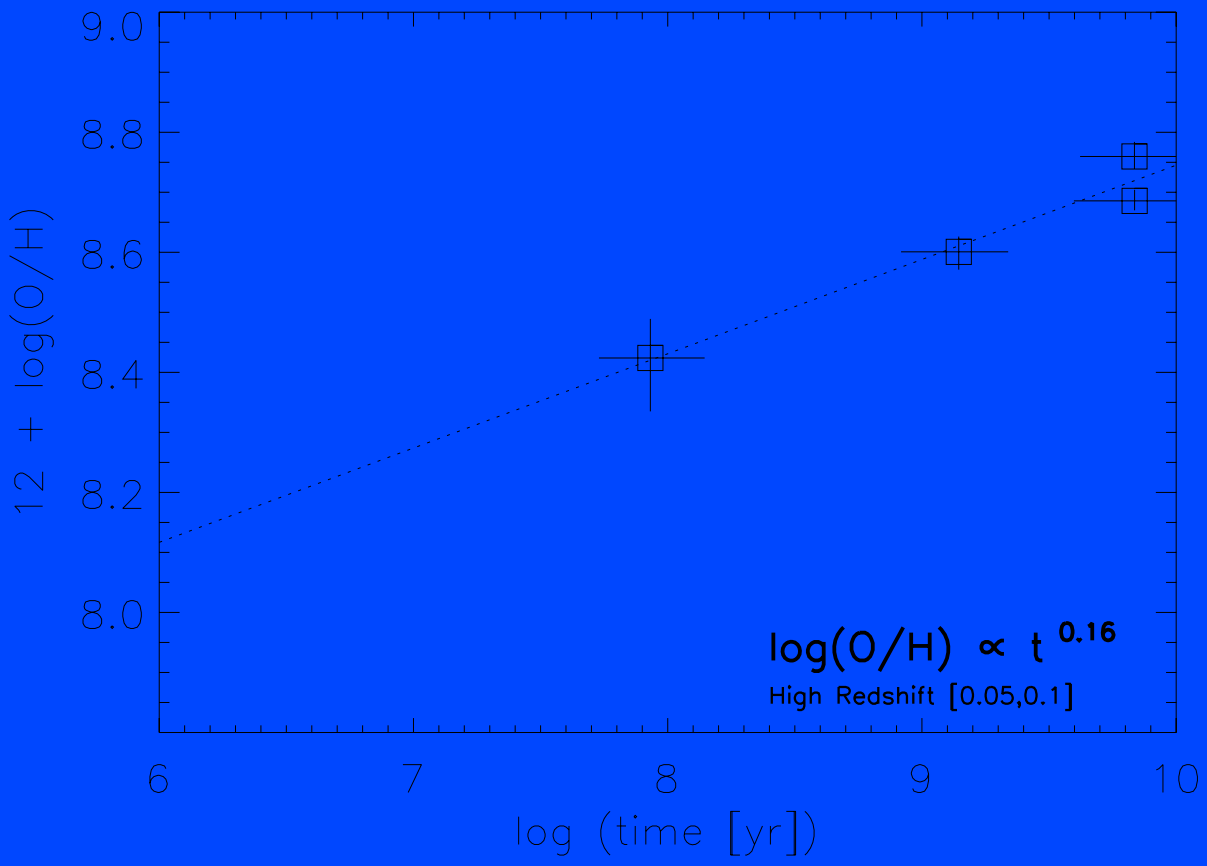


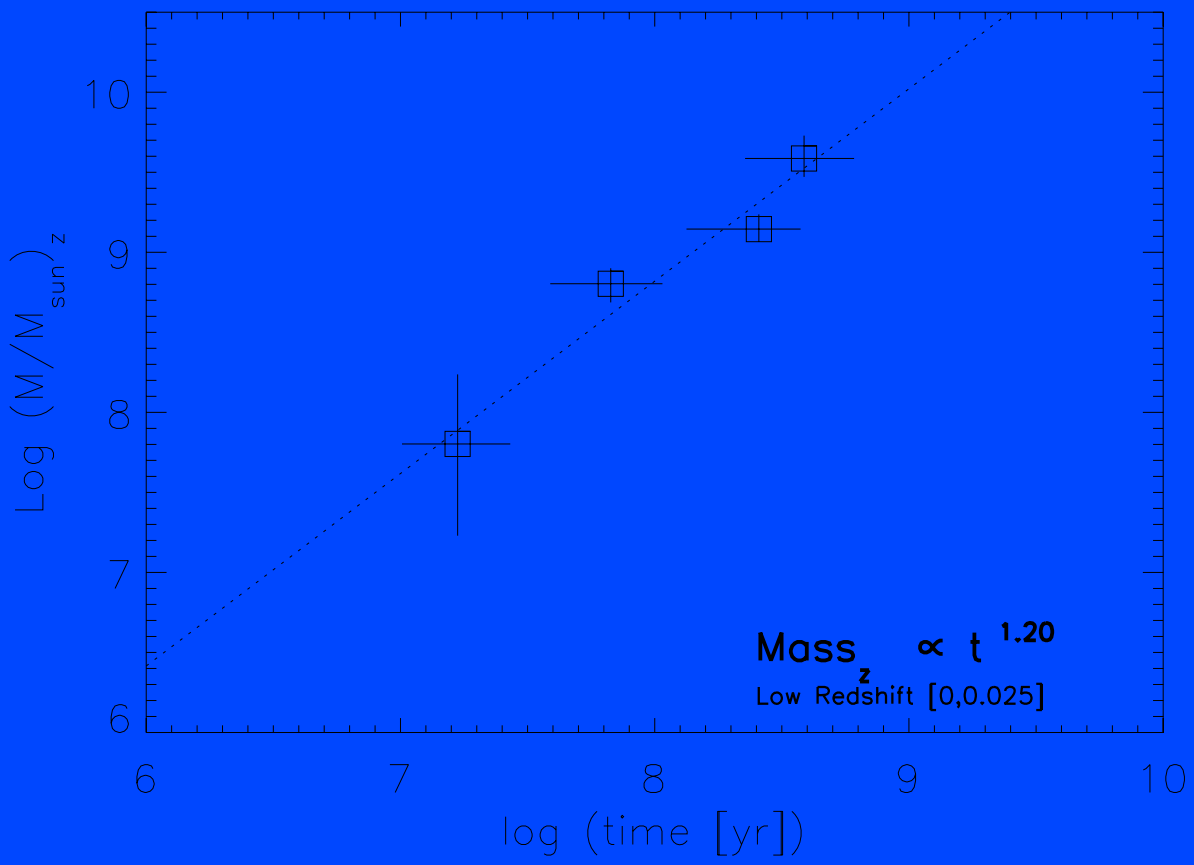

Figure 1: Low (left), medium (center) and high (right) redshift distributions

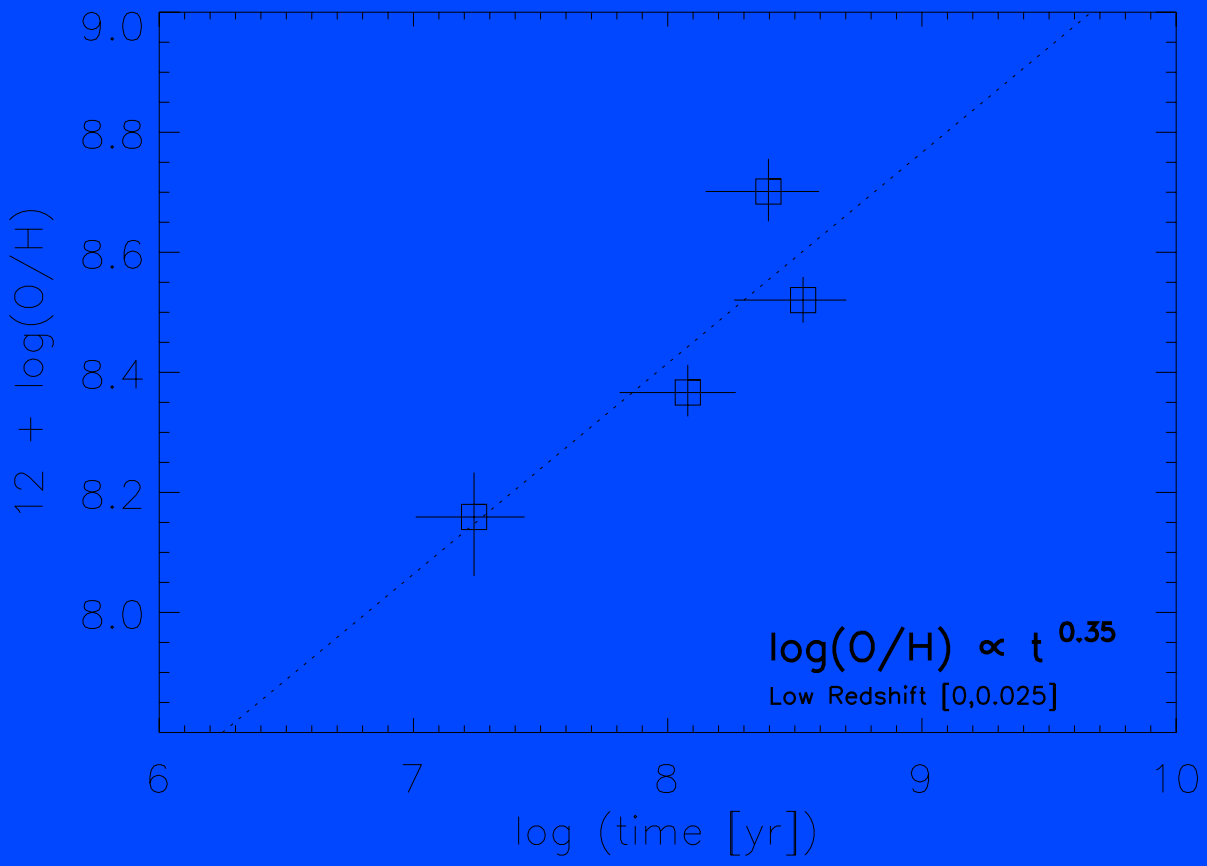

Log (M/M$_{sun}$)$_z$
10
9
8
7
6
6
7
8
9
10
log (time [yr])
Mass$_z$ ∝ t$^{0.48}$
Medium Redshift [0.025,0.05]


Log (M/M$_{sun}$)$_z$
10
9
8
7
6
6
7
8
9
10
log (time [yr])
Mass$_z$ ∝ t$^{0.33}$
High Redshift [0.05,0.1]


9.0
8.8
8.6
8.4
8.2
8.0
12 + log(O/H)
6
7
8
9
10
log (time [yr])
log(O/H) ∝ t 0.19
Medium Redshift [0.025,0.05]


9.0
8.8
8.6
8.4
8.2
8.0
12 + log(O/H)
6
7
8
9
10
log (time [yr])
log(O/H) ∝ t 0.16
High Redshift [0.05,0.1]


Log (M/M_sun)_z
10
9
8
7
6
6
7
8
9
10
log (time [yr])
Mass_z ∝ t^1.20
Low Redshift [0,0.025]


9.0
8.8
8.6
8.4
8.2
8.0
12 + log(O/H)
6
7
8
9
10
log (time [yr])
log(O/H) ∝ t 0.35
Low Redshift [0,0.025]

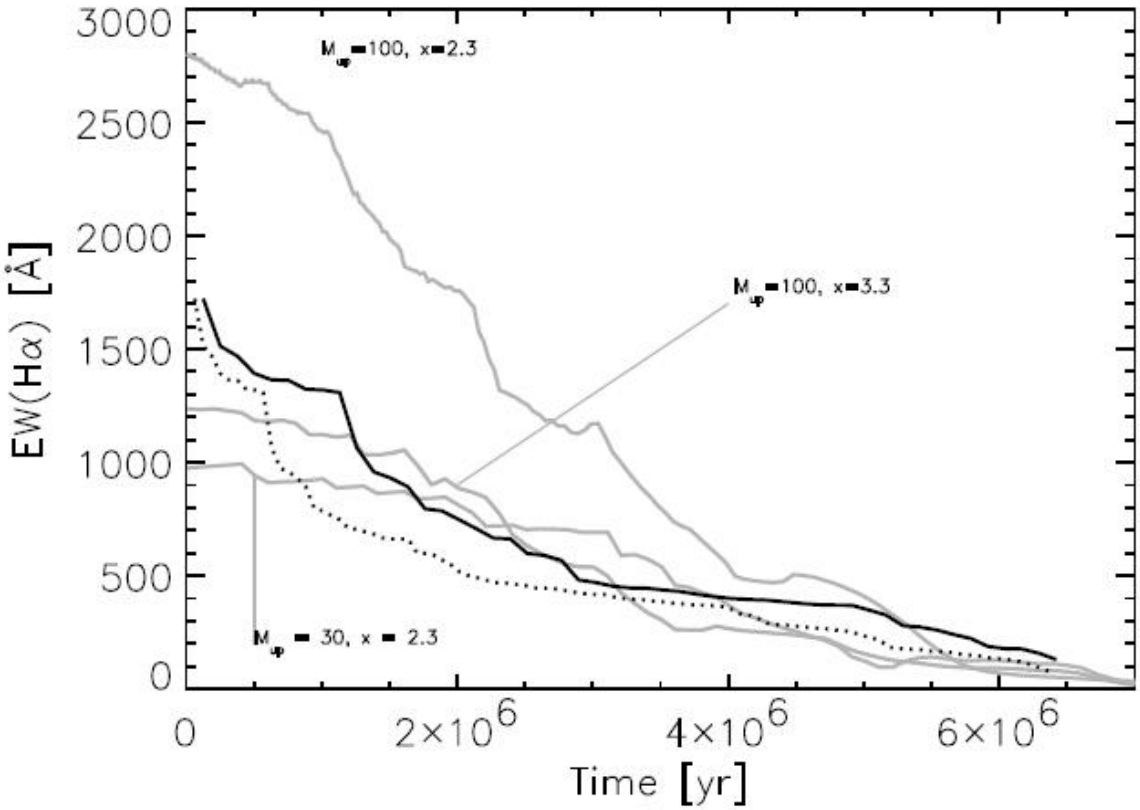



**Figure 3.19:** Restricted metallicity inversions compared with SB models (grey lines). Inversions are for the 50 (solid black line), and the 100 lowest metallicity objects (dotted black line).

# Slope of the SFR vs AGE

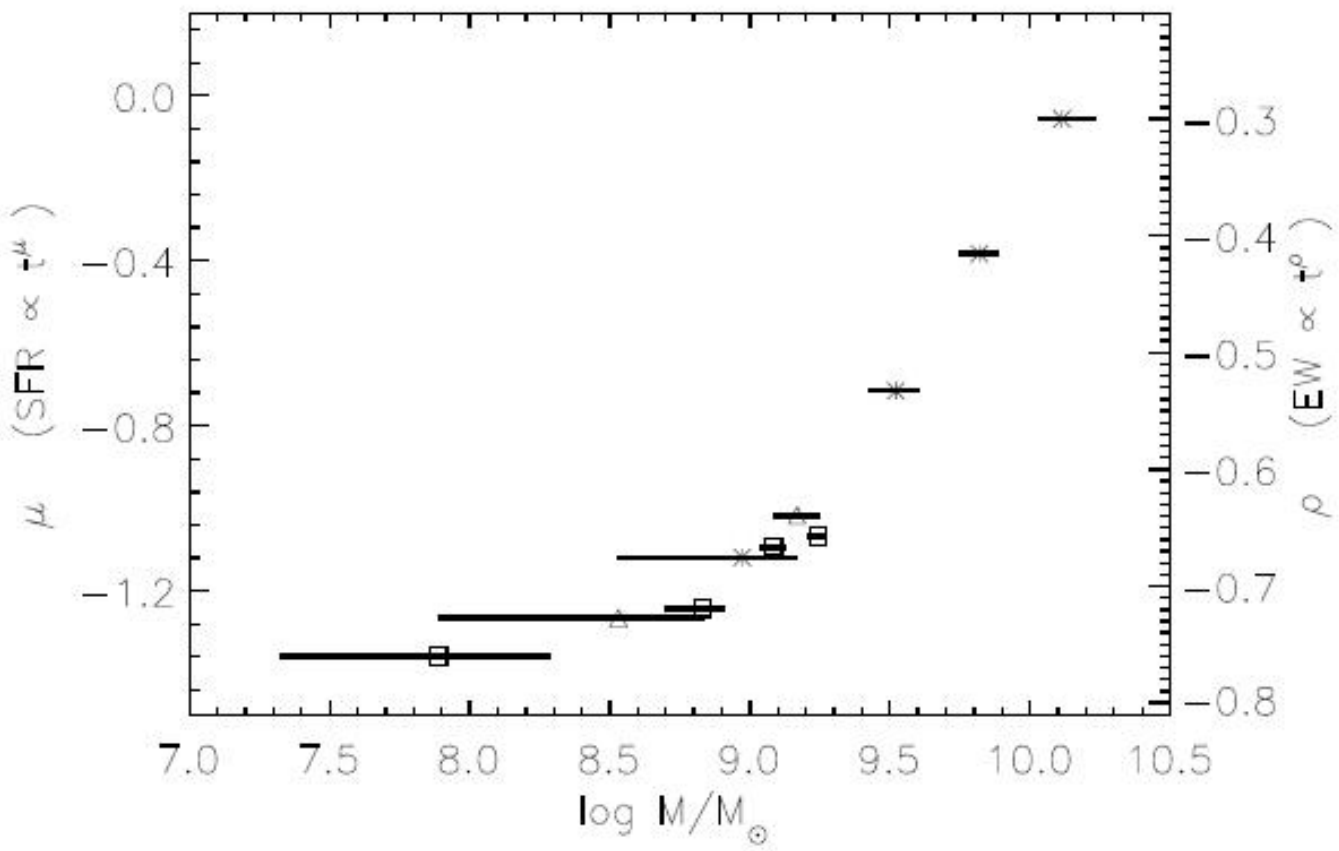



**Figure 4.17:** SFR ($\mu$) and EW ($\rho$) power law indices as a functions of mass. Bins $a, b, c$ and $d$ from figure 4.12 correspond to asterisk symbols. Bins from figure 4.14 correspond to squares. The horizontal lines show the extent from the second to the third quarter (central 50 % of the distribution), the symbol indicates the median for each mass bin.

# Extremely low metallicity range

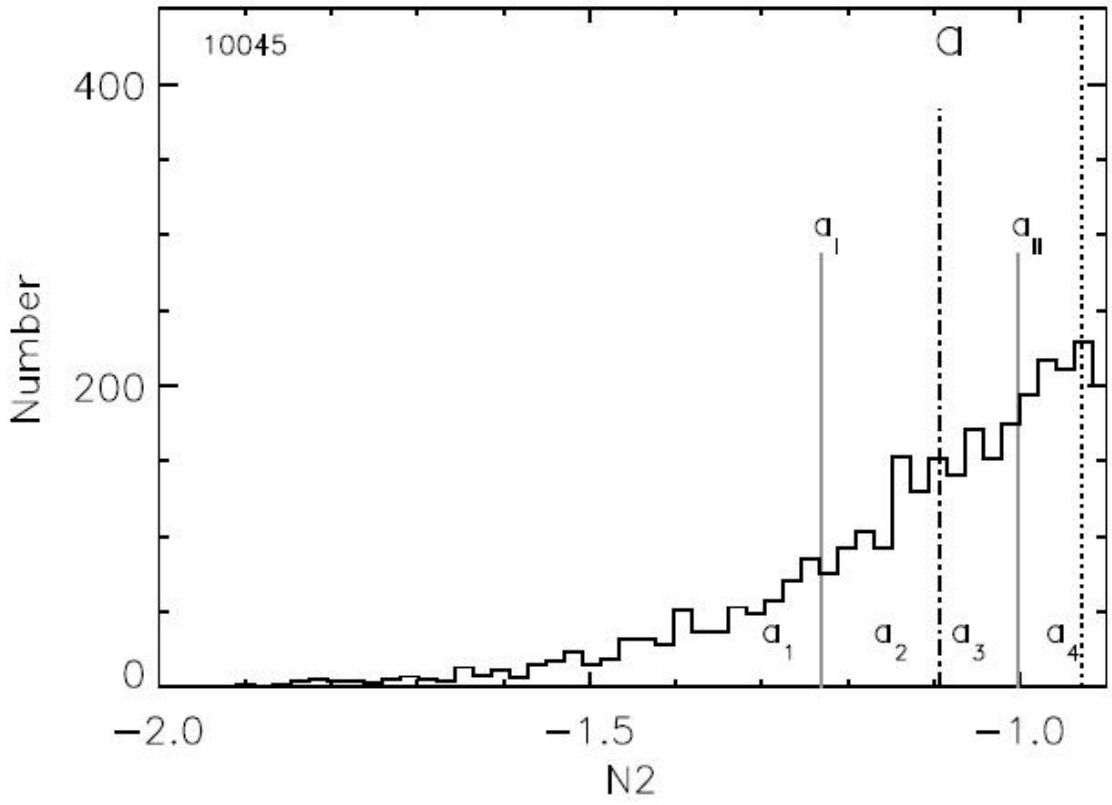
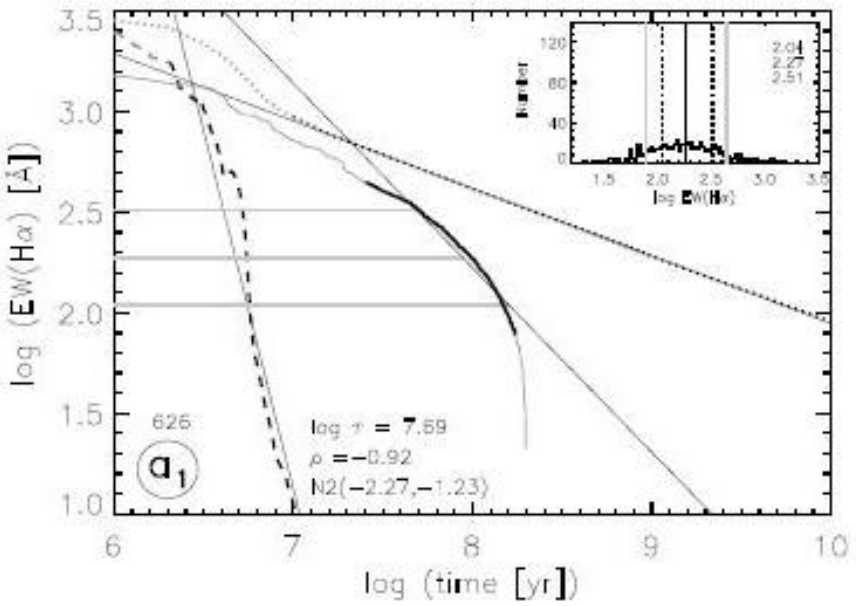
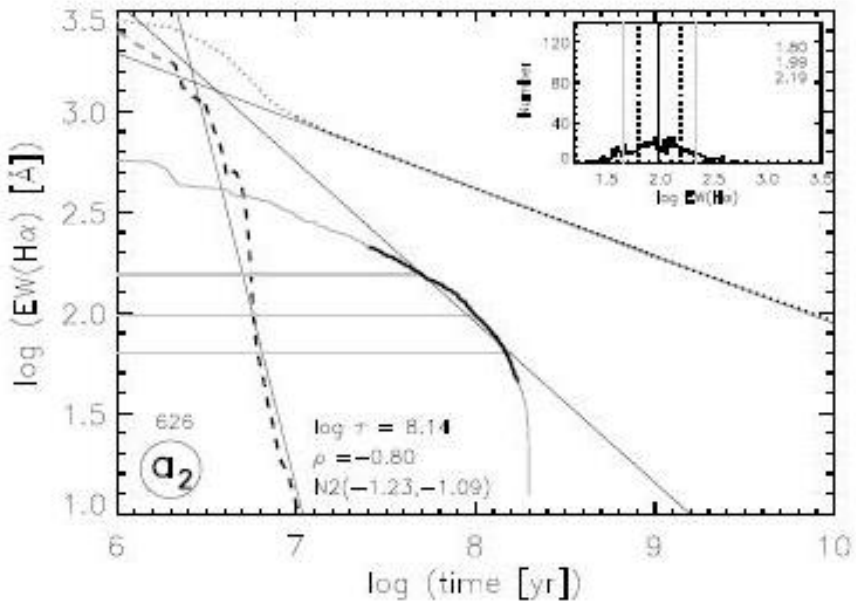
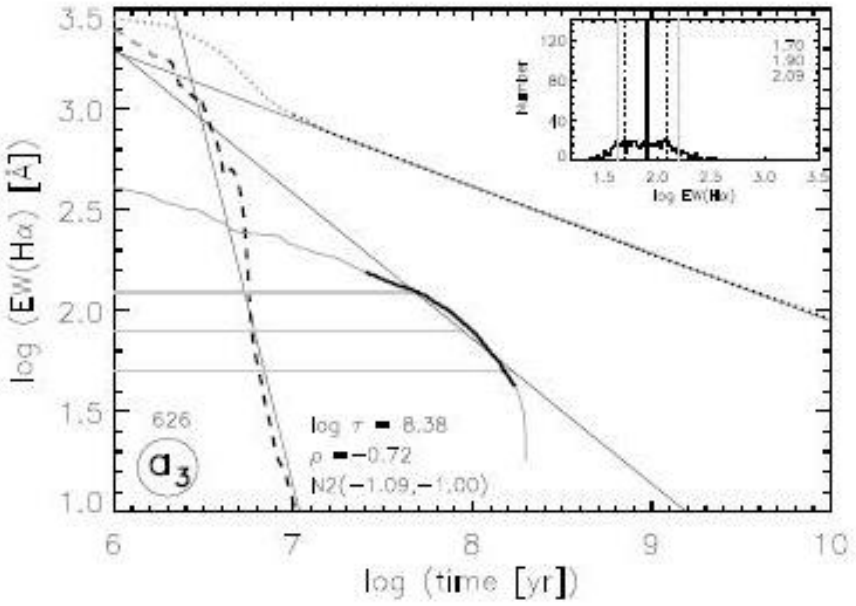



**Figure 3.16:** The lowest metallicity quarter from figure 3.14 was sub-divided in two ($a_I$ and $a_{II}$) and four sections ($a_1, a_2, a_3$ and $a_4$) of equal number each.

# Extremely low metallicity dependence



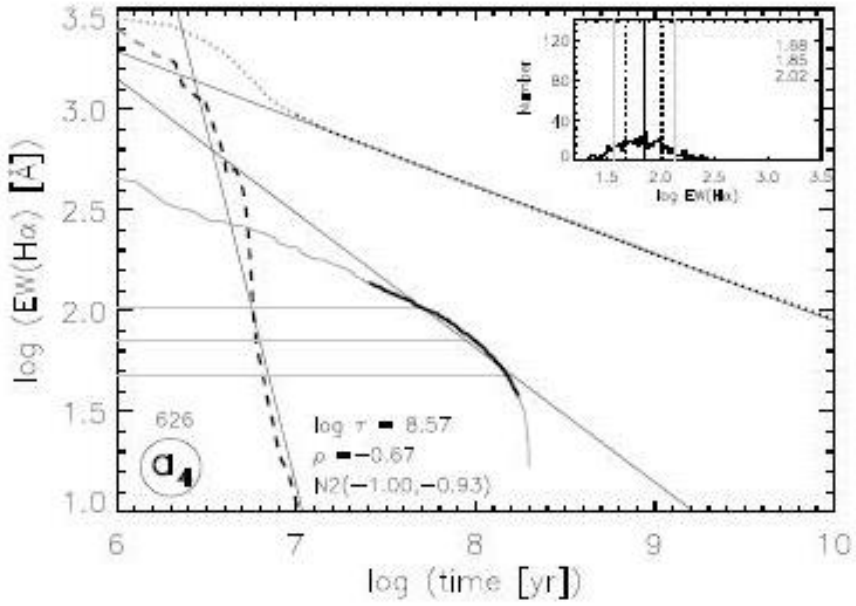




**Figure 3.18:** Inversion for data subsets of increasing metallicity. The letters correspond to the bins $a_1, a_2, a_3$ and $a_4$ in figure 3.16.